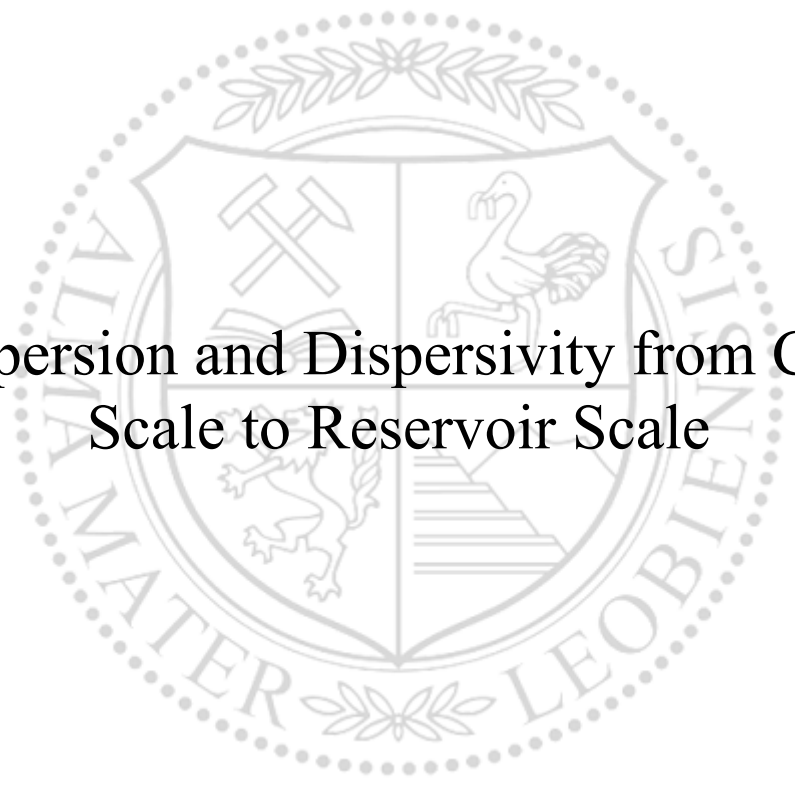




Chair of Reservoir Engineering

Master's Thesis



Dispersion and Dispersivity from Core
Scale to Reservoir Scale

Eleonora Pechorskaya

May 2019

This study is dedicated to my mother who has given me the ground for being an intellectually developed personality, curious and ambitious. I would like to thank her for her words of encouragement when the difficulty seemed too much. I also would like to dedicate this work to my grandparents who have never stopped believing in me. The last, but not the least, I am dedicating this work to David Böck who supported me morally throughout all my study, gave me good advice and help.



AFFIDAVIT

I declare on oath that I wrote this thesis independently, did not use other than the specified sources and aids, and did not otherwise use any unauthorized aids.

I declare that I have read, understood, and complied with the guidelines of the senate of the Montanuniversität Leoben for "Good Scientific Practice".

Furthermore, I declare that the electronic and printed version of the submitted thesis are identical, both, formally and with regard to content.

Date 30.04.2019

A handwritten signature in blue ink, appearing to read 'Eleonora Pechorskaya'.

Signature Author
Eleonora, Pechorskaya
Matriculation Number: 11703469

Acknowledgements

I would like to thank Gisela Vanegas Cabas, Dominik Steineder and Torsten Clemens who were more than generous with their expertise and precious time in their guidance as my supervisors. Their willingness to give me feedback whenever I had any question made this research an enjoyable and fruitful experience. Moreover, I really hope that they will enjoy reading it even more than I enjoyed putting it together.

It is very important for me to acknowledge OMV Exploration & Production GmbH for allowing me to conduct my research and providing me with all the necessary hardware, software, and supervision. Their support with all organizational and technical issues helped me to focus fully on my thesis.

Finally, I would like to thank my university professor Holger Ott who agreed not only to be my evaluator but also my supervisor. His clever remarks helped me to get another point of view on the topic.

Abstract

Upstream companies nowadays are widely using chemical floods to achieve incremental oil production. However, before the company makes the decision of implementing the flood on the field, a number of simulation forecasts are done to estimate the possible oil recovery. The reliability of the forecasts is studied in this work with the focus on the influence of dispersion on the forecast results.

Influence of dispersion on the fluid flow in porous media is a well-known fact, it should therefore also be introduced in the flow simulation. This is possible by mimicking the actual, physical dispersion by numerical dispersion. Numerical dispersion, or “truncation error”, is an artifact of the current simulation techniques that may lead to severe distortions along with an occurrence of rapid saturation changes.

The role of gridding and the size of calculation time-steps for different types of models (1D/2D domain with single/two-phase flow) is studied. These models were created with Petrel and simulation runs done in Eclipse – both Schlumberger Ltd. software. The dispersion was calculated by analyzing tracer-concentration and production-rate curves.

While time-step size had a significant impact on all the homogeneous models, gridding was the important issue in terms of tracer production for both types of models: homogeneous and heterogeneous. The influence of gridding on dispersion led to an underestimation of incremental oil-recovery after the alkali-polymer flood, even though the influence of gridding on the water-cut was insignificant.

An alternative technique of influencing numerical dispersion is the introduction of relative-permeability pseudo-function to match the water-cut (the volumetric ratio of water production to total liquid). However, the increase of the gridding by a factor of 20 still resulted in a very good water-cut match, and that left very little room for improvement. The only one relative-permeability pseudo-function that maintained the quality of the match, did not bring any improvements on the tracer curve match.

Another technique available in Eclipse to control numerical dispersion is the “diffusion control” option. The usage of that option led to maintaining the water-cut match quality while improving the tracer production-curve match. The improvement of the tracer production curves match might lead to the improvement of forecasts of incremental oil-recovery after the alkali-polymer flood.

Zusammenfassung

Erdölfördernde Unternehmen verwenden heutzutage vermehrt Polymer- und Tensidfluten, um die Ausbeute der Lagerstätten zu erhöhen. Bevor diese Verfahren im Feld angewendet werden, wird in der Regel eine Vorhersage der zusätzlichen Fördermenge durch Simulationen durchgeführt. Die Zuverlässigkeit dieser Vorhersagen wird in dieser Arbeit untersucht, wobei der Fokus auf die Auswirkung von Dispersion auf das Resultat gelegt wird.

Der Einfluss von Dispersion auf das Strömungsverhalten von Flüssigkeiten in porösen Materialien ist bekannt, und sollte in numerischen Simulationen berücksichtigt werden. Die Abbildung der "tatsächlichen Dispersion" kann durch Manipulation der sogenannten numerischen Dispersion erreicht werden. Numerische Dispersion, auch Diskretisierungsfehler genannt, entsteht durch die derzeitig verwendeten numerischen Lösungsverfahren, und kann zu starken Verfälschungen und Abweichungen führen, wie zum Beispiel das Auftreten sehr schneller Sättigungsänderungen.

Der Einfluss der Zellblock-Größe und des Berechnungs-Zeitschrittes wurde für verschiedene Arten von Modellen (1D/2D Domänen mit Ein-/Zweiphasenströmung) untersucht. Diese Modelle wurden mit Petrel erstellt und mit Eclipse simuliert (Beide Programme von Schlumberger Ltd.). Die Dispersion wurde anhand von Tracer-Konzentrations- und Förderungsratendiagrammen berechnet.

Die Größe der Zeitschritte hatte einen Einfluss auf alle homogenen Modelle, wohingegen die Zellblock-Größe einen maßgeblichen Einfluss auf die Tracer-Förderungsrate sowohl in den homogenen als auch den heterogenen Modellen hatte. Der Einfluss der Zellblock-Größe führte zu einer zu niedrigen Vorhersage der zusätzlichen Erdölförderung nach der Alkali-Polymer Injektion, der Einfluss auf den geförderten Wasseranteil war vernachlässigbar.

Eine alternative Möglichkeit die numerische Dispersion zu beeinflussen ist die Verwendung von Pseudo-Funktionen für die relative Permeabilität um den Wasseranteil bzw. die Wasserförderung besser anzugleichen. Da aber die Erhöhung der Zellblock-Größe um einen Faktor von 20 noch immer zu einem sehr guten Match des Wasseranteils führte, blieb wenig Raum zur Verbesserung. Nur eine der verwendeten Pseudo-Funktionen führte zu keiner Verschlechterung des Wasseranteil-Matches, sie brachte jedoch keine Verbesserung des Tracer-Matches

Eine weitere Möglichkeit, die numerische Dispersion in Eclipse zu beeinflussen ist die Option „Diffusion Control“. Die Verwendung dieser Option änderte nichts an dem Match des Wasseranteils, verbesserte jedoch den Tracer-Match.

Eine Optimierung des Tracer-Matches könnte in weiterer Folge zur Verbesserung der Vorhersage der zusätzlichen Erdölförderung führen.

Table of Contents

Chapter 1	Introduction.....	11
1.1	Background and Context.....	11
1.2	Scope and Objectives.....	13
1.3	Achievements.....	14
1.4	Overview of Thesis.....	14
Chapter 2	Literature Review.....	17
Chapter 3	1D model.....	21
3.1	Single-phase flow, tracer in water.....	21
3.2	Multi-phase (oil and water) flow.....	26
Chapter 4	2D model.....	35
4.1	Geological background and introduction of heterogeneity.....	35
4.2	Two-phase flow (oil and water).....	52
4.3	Two-phase flow with alkaline-polymer.....	56
Chapter 5	History matching.....	58
5.1	Relative-permeability pseudo-functions.....	58
5.2	Diffusion control.....	60
Chapter 6	Results and Discussion.....	63
6.1	1D homogeneous single-phase flow models.....	63
6.2	1D homogeneous two-phase flow models.....	63
6.3	2D homogeneous single-phase flow models.....	64
6.4	2D heterogeneous single-phase flow models.....	64
6.5	2D two-phase flow models.....	65
6.6	History match.....	66
Chapter 7	Conclusion.....	67
7.1	Summary.....	67
7.2	Evaluation.....	67
7.3	Future Work.....	67
	List of Figures.....	69
	List of Tables.....	71
	References.....	72

Nomenclature

α	Dispersivity	[m]
D_L	Longitudal dispersion	[m ² /s]
C	Concentration	dimensionless
V	Velocity	[m/s]
L	Distance	[m]
t	Time	[s]
D_m	Molecular diffusion	[m ² /s]
Δx	Grid-block size in x-direction	[m]
ϕ	Rock Porosity	dimensionless
μ	Fluid Viscosity	[Cp]
k	Permeability	[mD]
Q	Total Flow Rate	[m ³ /day]
ρ	Fluid Density	[kg/m ³]
σ_{ow}	Interfacial Tension	[N/m]
Nc	Capillary Number	dimensionless
Pe	Péclet number	dimensionless

Abbreviations

EOR	Enhanced Oil Recovery
C/D	Convection-Dispersion
CDE	Convective-Dispersion Equation
Ngb	Number of Grid-Blocks
PV	Pore Volume
SP	Spontaneous Potential
TH	Tortonian Horizon
TGS	Truncated Gaussian Simulation
AP	Alkaline-polymer

Chapter 1 Introduction

The role of dispersivity is important in alkaline-polymer flooding and conducting an investigation on this topic enables us to contribute to the predictions of the possible success of alkaline-polymer flood. The scope of this thesis is to study the numerical dispersion and dispersivity in porous media along with the physical dispersion, mainly its impact on the tracer production curves and oil incremental production, by performing various numerical simulations.

1.1 Background and Context

In this thesis, dispersion is referred to as the spreading phenomena of a tracer volume in a porous medium due to velocity gradients along the path, mechanical mixing in the pores and heterogeneity (Bear 1972; Lake 1989), whereas dispersivity is an empirical rock-fluid property that determines the characteristic dispersion of the medium through the following correlations:

$$D = \alpha \cdot V + D_m \quad (1.1.1)$$

$$V = \frac{L}{t} \quad (1.1.2)$$

In the equations above, D stands for dispersion coefficient, α for dispersivity, V for velocity, which is derived through L that expresses the distance that the tracer has travelled, and t for the time it took the tracer to travel. D_m stands for molecular diffusion coefficient.

Dispersion is a non-steady, irreversible process. In total, Bear (1972) listed six origins of dispersion:

1. Pore network microscopic geometry;
2. External forces that act on the liquid;
3. Variations in liquid properties (viscosity, density and etc.);
4. Molecular diffusion;
5. Liquid and solid phases interaction (sorption);

6. Chemical and physical processes that lead to changes in tracer concentration.

Molecular diffusion is neglected in this work, as the diffusion base *Péclet number* (Pe) is greater than one. In other words, the convection effects are greater than the diffusion effects in terms of determining the overall mass flux. Systems that are larger than micrometer scale normally have this kind of overall mass flux determination.

$$Pe = \frac{Lv}{D_m} \quad (1.1.3)$$

Where L stands for the characteristic length scale, v stands for the velocity magnitude, and D is a characteristic diffusion coefficient.

The length of the simulated core (Figure 6) is 0.291 meters. The interstitial velocity of the tracer was within the range $2.08 \cdot 10^{-6}$ - $1.7 \cdot 10^{-5}$ m/s. Therefore, for the *Péclet number* to be smaller than one, D_m should be greater than $6.05 \cdot 10^{-7}$ m²/s, whereas the typical range of the diffusion coefficient for water solutions is 10^{-10} to 10^{-9} m²/s.

As the Pe is greater than one, the diffusion effects can be neglected for the purpose of this master thesis' investigation, as on the macroscopic scale diffusion is extremely slow, and the dispersion coefficient can be written:

$$D = \alpha \cdot V \quad (1.1.4)$$

In the calculation of dispersion of real field-example diffusion was also neglected as for a 162m flow distance diffusion effects are insignificant.

“Numerical dispersion” is a phenomenon that is different from the described above dispersion, as it has no physical background. In some literature, it is even addressed as “truncation error”. In fact, it is an artifact of the current numerical simulation techniques. This artifact causes severe distortions in which rapid saturation changes occur.

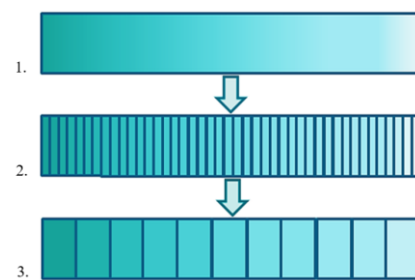


Figure 1. Saturation averaging in a cell

Figure 1 displays the saturation averaging process. The first rectangle represents the core plug. The dark green color on the left side indicates a high water saturation, while the white color on the right side indicates a high oil saturation. In the second rectangle, the core plug is split into a number of sections of equal length. To find the saturation of each grid cell in the simulation model, the saturations of three of these sections are taken and averaged. This is represented by the third rectangle. As can be seen, this averaging has a strong influence on the production

characteristics of the model: While the high oil saturation on the right in the actual plug would have lead to an initial production of only oil, there is no such high oil saturation in the simulation model, and that leads to earlier water-breakthrough.

In addition to the rapid saturation changes caused by numerical dispersion, the comparison of various tracer-concentration production curves and various tracer cumulative production curves proves the increasing smearing out at tracer front due to the increase of truncation error. The improvement in the tracer production-rate match may give the industry the chance to have improved oil-recovery forecasts after the alkaline-polymer flood.

1.2 Scope and Objectives

The main scope of this work is to investigate how to mimic physical dispersion with numerical dispersion. These types of investigations have already been done in a number of simulation studies. However, it was never investigated if numerical dispersion has an impact on the incremental oil-recovery forecasts after the alkaline-polymer flood. The forecast is the key to the evaluation of the economic efficiency of EOR projects, before implementing them. In case of an inaccurate forecast, a wrong decision may be made concerning alkaline-polymer project implementation.

The best-known strategy to influence on the numerical dispersion is to adjust grid-block size and calculation time-step size. However, while for relatively small core models it is easy to set up a simulation model with grid-block size in a millimeter range and a calculation time-step size of several seconds, for a field scale model it is impossible. Therefore, the industry should come up with other ideas on how to operate with numerical dispersion and dispersivity.

The main focus was put into the investigation of parameters that influence the total dispersion (physical and numerical) in the simulated models: grid-block size, calculation time-step size, porosity, core-plug/field saturation state, oil viscosity, relative-permeability functions.

The investigation was done on several types of models:

- 1D homogeneous single-phase flow models
- 1D homogeneous two-phase flow models
- 1D homogeneous models of alkaline-polymer flooding
- 2D homogeneous single-phase flow models
- 2D homogeneous two-phase flow models
- 2D heterogeneous single-phase flow models
- 2D heterogeneous two-phase flow models
- 2D heterogeneous models of alkaline-polymer flooding

The data for the 1D model was taken from a Bentheimer core-plug tracer-test, which was already performed by OMV. The performed simulation set up for the tracer-test history-match was taken as the starting point for the investigation of dispersion and dispersivity in the 1D domain.

The 2D models were created on the basis on actual well-logs (mainly SP-logs), seismic and core data. The thickness of the model is almost the same along the investigated distance (162 m between the main injection and production wells). The petrophysical properties of the model could be called relatively homogeneous. More detailed information of the geological model is given further in the chapter devoted to 2D models.

1.3 Achievements

Right now, it is challenging to reproduce physical dispersion by the numerical one. Changing the grid block size to the minimum that will not break the limit of cost and time would help to control numerical dispersion. In addition, it was observed that the direction in which grid-block size is increased should be also chosen carefully: the grid block should be decreased in the lateral direction, and it is better to keep the grid block as big as log-data resolution (down to 15 cm) in the vertical direction.

In the homogeneous model, the calculation time step-size has a huge impact on numerical dispersion. Obviously, by using the smallest possible time step, the resulting numerical dispersion will be decreased. In heterogeneous models, the situation cannot be changed by the reduction of the time step, as the heterogeneous effect highly dominates (the real dispersion is so much bigger).

Introducing relative permeability pseudo functions is very helpful in reproducing the water-cut behavior. The idea of this approach is to sharpen the saturation front.

A noticeable effect of single-phase flow in the 2D heterogeneous model was the fact that the tracer production profile in 162 m distance from the production well is more symmetrical than at the 54.5 m distance.

Another interesting investigation was the simulation of the alkaline-polymer flood, which showed an underestimation of oil recovery after the chemical flood by using grid blocks with a size in the x-direction of 20 m compared to 1 m grid blocks.

1.4 Overview of Thesis

In various hydrogeology studies, field, and core-plug tracer-tests, numerical simulations have been focused on the dispersion phenomenon. The results of those studies sometimes verified

each other, sometimes were in contradiction with each other. Chapter 2 is summarizing these studies and presents the state of the art knowledge on physical and numerical dispersion and dispersivity.

Chapter 3 is discussing the effects of total (physical and numerical) dispersion in 1D models and giving the description of the model simulation set-up. The way Eclipse treats alkaline-polymer flood is also described in the first chapter, along with the used keywords.

Chapter 4 starts with the description of the 2D geological model: reservoir geological background, distribution of the petrophysical properties and the upscaling. While chapter 3 is a validation of already published results, the description of the investigated correlations that were caused by real and numerical dispersion in a heterogeneous environment in chapter 4 is not so obvious, as dispersion in a complex flow field is not so well understood in the industry.

While investigating truncation error of the flow in the 2D heterogeneous medium simulation it is important to understand the consequences of upscaling, due to that chapter 4 is observing how it affects tracer production-rate and the forecast of additional oil-recovery after the alkaline-polymer flood. The last-mentioned is the most interesting part for the industry. The most important number for the management for the decision of applying EOR is the additional recovery factor. The project might not proceed if the forecasts gave too low additional production. However, the recovery factor might be miscalculated (over- or underestimated) due to the numerical effects in the simulations. This was the reason for the comparison of the fine and coarse reservoir model simulation of a chemical flood, which gave an underestimation of the recovery factor while using the typical for simulations grid block size.

In some situations, reservoir engineers can not decrease the grid-block size of a model. These situations can be caused by limited computing resources or time constraints. Chapter 5 describes solutions to improve the history-match of tracer production curves in these situations.

The last chapters provide an overview of the results, their discussion, and conclusions.

Chapter 2 Literature Review

The fundamental works concerning dispersion were worked out in the second half of the twentieth century. Taylor (1953) described tracer dispersion in laminar Newtonian flow in long capillary tubes (Figure 2). The flow velocity varies over the cross-section of a tube: the part of the injected fluid that was initially near the center of the tube is carrying tracer particles faster than the part which was initially near the wall.

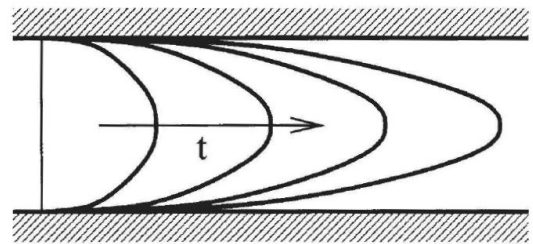


Figure 2. Tracer displacement of a resident fluid in a capillary tube of circular cross-sectional area πR^2 .

Taylor (1953) stated that in a tube of radius R and maximum fluid velocity u_0 , the velocity u at distance r from the tube's centre is:

$$u = u_0 \left(1 - \frac{r^2}{R^2}\right) \quad (2.5)$$

However, this is only valid if dispersion is caused only by convection ($D_m = 0$).

In his experiments, the mean value of the concentration over a cross-section of a tube (C_m) is defined by:

$$C_m = \frac{2}{R^2} \int_0^R C r dr \quad (2.6)$$

Where C is the concentration is a function of the travelled distance (x), velocity (u), time (t) and distance from the tube's centre (r):

$$C = f(x - ut, r) \quad (2.7)$$

De Josselin de Jong (1958) describes random porous media: it is medium with a series of interconnected straight channels of equal length, orientated at random, uniformly distributed in all directions, in which average uniform flow takes place. He assumes that, within each channel, tracer particle moves with a mean velocity in a radial diffusion pattern.

A number of works similar to the studies of de Josselin de Jong (1958) concluded that the longitudinal (D_L) and transversal (D_T) dispersion values are proportional to the mean velocity and to the length of the elementary canals. Those canal sizes are in the order of grain sizes. Therefore, with the increase of the mean travel distance, the ratio between D_L and D_T increases.

The last statement is in contradiction to the work of Blackwell (1959). He published that this ratio is dependent on the mean velocity only and independent of the distance travelled by the tracer.

However, de Josselin de Jong was the first one to describe a distinct difference between longitudinal and transverse dispersions. Over the years, scientists learned that the ratios between longitudinal and transversal dispersion differ widely.

The basis of calculating dispersivity is the convection-dispersion equation, which governs fluid transport in porous media. Pickens and Grisak (1981) expressed the general, three-dimensional convective-dispersion equation with the assumption of a one-phase incompressible flow with no chemical reactions, constant porosity, and negligible adsorption as:

$$\frac{\partial c}{\partial t} + \nabla \cdot c\vec{v} - \nabla \cdot (\vec{D} \cdot \nabla c) = 0 \quad (2.8)$$

Here \vec{D} stands for the dispersion tensor, \vec{v} is the vector for interstitial velocity, c is the concentration of solute.

The one-dimensional form of the equation is:

$$\frac{\partial c}{\partial t} + v \frac{\partial c}{\partial x} - D \frac{\partial^2 c}{\partial x^2} = 0 \quad (2.9)$$

The mathematical approach of Ogata and Banks (1961) for the 1D tracer production concentration dispersion was used in this thesis, where D_L stands for the longitudinal dispersion:

$$c(x, t) = \frac{c_j}{2} \left[\operatorname{erfc} \left(\frac{x - v_x t}{2\sqrt{D_L t}} \right) + e^{\frac{v_x t}{D_L}} \operatorname{erfc} \left(\frac{x + v_x t}{2\sqrt{D_L t}} \right) \right] \quad (2.10)$$

This equation is the 1D solution for the convection-dispersion equation. It uses the complementary error function, $\operatorname{erfc}(x)$, and is defined by:

$$\operatorname{erfc}(x) = 1 - \operatorname{erf}(x) = 1 - \frac{2}{\sqrt{\pi}} \int_0^x e^{-t^2} dt = \frac{2}{\sqrt{\pi}} \int_x^{\infty} e^{-t^2} dt \quad (2.11)$$

The error function and the complementary error have the following shapes:

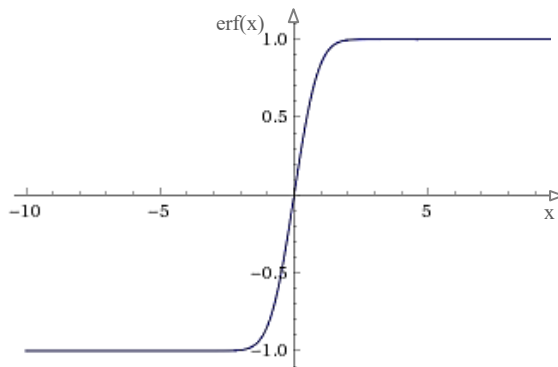


Figure 3. Error function

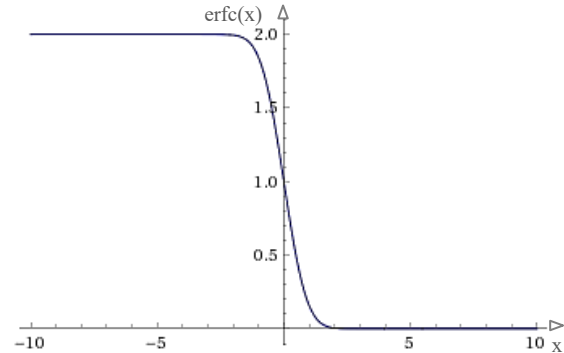


Figure 4. Complementary error function

Larry W. Lake has a vast number of papers published on related topics. Chapter 3 of the thesis that was devoted to homogeneous 1D model proved the correlations stated in his report “A systematic procedure for reservoir characterization”. There he comes up with a solution on how to find the actual dispersion of a 1D homogeneous system with one phase flow by running a series of simulations of different gridding size. However, this solution does not help with getting rid of the numerical dispersion during the simulation, to get the proper results for production. We can only estimate how wrong the results are.

In 1972, Bear published in his book that dispersivity is a constant of every distinct permeable medium. Further works (simulations and core experiments) proved that dispersivity is also a scale-dependent property (Arya et al. 1988; Garmeh et al. 2009; Jha et al. 2009; John et al. 2010; Mahadevan et al. 2003; Lake 2013; Pickens and Grisak 1981).

No confident statements concerning this question are present from field-scale experiments. Gelhar et al. (1992) have referred data from 59 fields to describe the scale effect of dispersion. The data in the paper was split into highly reliable, intermediate reliability and low reliability.

To be classified as high-reliability, *all* of the following criteria had to be fulfilled:

- Well defined tracer input, i.e. both the input concentration and injection schedule must be known
- The tracer must have been conservative, i.e. non-reactive with no physical interaction due to the particle sizes
- The spatial measurement of the tracer concentration was suited to the type of injection. For example, a three-dimensional measurement for injection into an aquifer, as tracer injection into an aquifer causes it to spread in all three dimensions

- An appropriate analysis of the tracer concentration was performed, e.g. breakthrough analysis

To be classified as low-reliability, *only one* of the following criteria had to be fulfilled:

- A single-well injection/withdrawal test was performed
- An unsuitable equation to calculate dispersivity was used
- An assumption of a perfectly stratified porous media was made
- The tracer input was not well defined

Without regard to reliability, they found a clear correlation of longitudinal dispersivity with scale. This trend is less clear when the data is classified according to reliability (Figure 5).

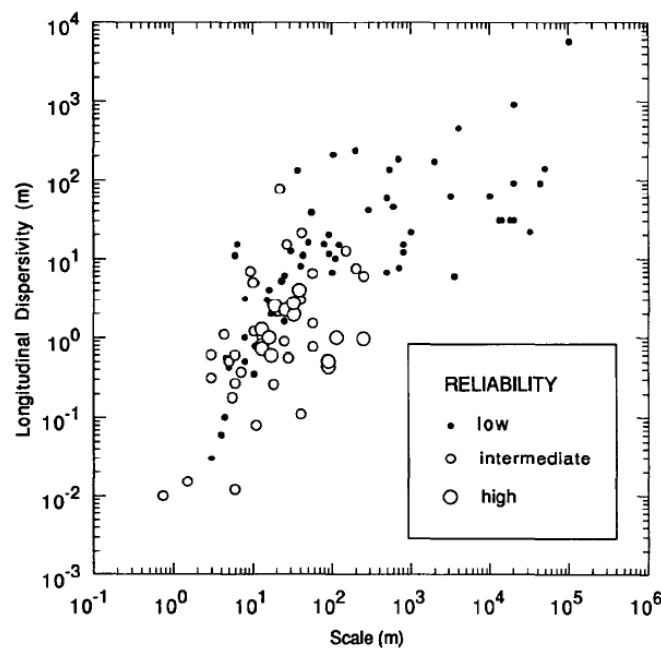


Figure 5. Longitudinal dispersivity versus scale with data classified by reliability (Gelhar et al. 1992).

Mainly in the papers, numerical dispersion stated to be larger than the real one (Lantz 1971; Haajizadeh et al. 1999). However, there is no literature available on exactly how big is the error in the 2D case, due to the sparse information on the dispersion in a highly complex flow field, especially when we talk about a highly heterogeneous media. While investigating truncation error of the flow in the 2D heterogeneous medium simulation it is important to understand the consequences of upscaling. The process of upscaling homogenizes the medium and that leads to the reduction of velocity variations in the coarse model comparing to the original, fine scale model. This reduction leads to less mixing in the upscaled case (Garmeh et al. 2009). On the other hand, the model with coarse grids has a higher truncation error than a fine-scale model

This thesis describes the effect of total dispersion in reservoir simulation for a realistic special case.

Chapter 3 1D model

Core-flood simulations discussed in this chapter investigate the dispersion and dispersivity through changing one of the listed variables per each simulation run:

- Porosity
- Permeability
- Cell size
- Time step size
- Tracer concentration
- Injection rate

In a two-phase flow core flood simulation, the change of dispersion and dispersivity with the change of average core saturation was studied. In addition, a simulation of high-viscosity oil was performed before proceeding to alkali-polymer flood.

Injection of passive (conservative) tracers, that have no influence on the flow, is simulated to avoid any chemical reactions in the investigations. Passive tracers do not change their properties with time. Tracer-production data is used to calculate dispersion by applying Ogata and Banks (1961) solution to the 1D solution of convection-dispersion equation (2.10).

In this study, time (t) input in equation (2.10) is the time when tracer production value is equal to half of the cumulative amount of the injected tracer

3.1 Single-phase flow, tracer in water

Before the simulations were started, OMV had already performed a history matching exercise for a first-contact miscible equal density displacement in a homogeneous permeable media. The resulting settings and core characteristics were taken as the starting point for the simulations.

Core-plug dimensions (Figure 6) are 29.1 centimeters in x-direction, 2.596 centimeters in y- and z-directions. This height and width were chosen to preserve the flow area from the real core

plug. The porosity of the core was set to 22%, and permeability was the same in all directions and equal to 1 362 mD.

Water viscosity was 0.5 cP at a reference pressure of 118.431 atmospheres, with water formation volume factor equal to 1.009 and water compressibility of $4.367e-005$ [atm^{-1}]. Water density at surface conditions was set to 1 g/cm^3 . To make the flow stable with no variations, the flow conditions were set to constant flow-rate boundary condition on both sides.

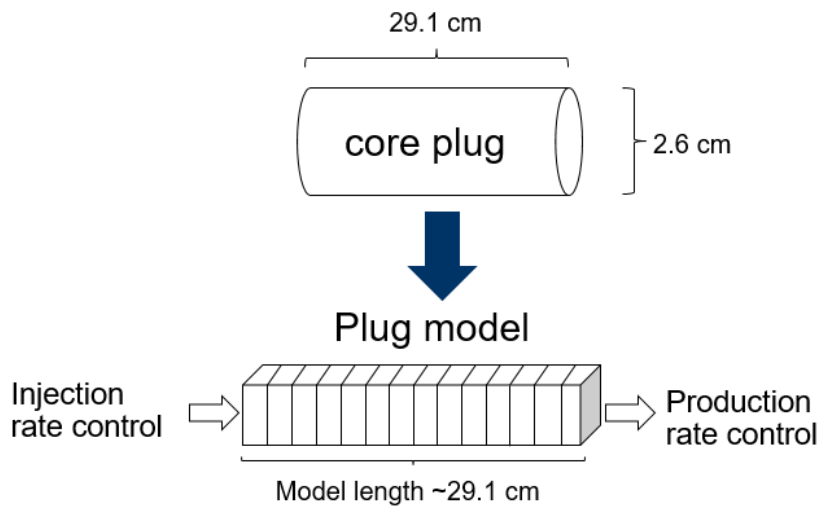


Figure 6. Core-plug dimensions

For every reservoir or core-flood simulations, one of the most time-consuming and difficult problems is the selection of a grid. The main considerations for grid selection are typically the following ones (Khalid Aziz, 1993):

- Geology and size of the reservoir
- Data available for reservoir description
- The desired numerical accuracy
- Objectives of the simulation study
- Location and type of wells
- Available software options
- Available time resources (constraints)

In the particular case of this study, the main consideration is the numerical accuracy, as we want to understand the impact of the numerical dispersion and how we can apply it for mimicking the real one.

The core tracer-test done by OMV gave the data for simulation history-match. As it was stated earlier in this section, the simulation set-up, which gave a high-quality history-match to this tracer test, was used as the starting point for the simulations in this chapter.

The simulation set-up had the following settings:

- 0.1 centimeter grid block size in x-direction
- 2.596 centimeters grid block size in y- and z-directions
- 0.01 seconds as the time step for calculations
- initialization by enumeration
- fully implicit formulation
- cartesian block centered grid
- black oil simulator (Eclipse 100)

In a one-dimensional flow, only longitudinal dispersion is present.

Table 1 describes how longitudinal dispersion (D), dispersivity (α) and interstitial velocity change with the change of porosity and grid-block length. Interstitial velocity is calculated using the equation (1.1.2).

Table 1. Summary of 1D homogeneous single-phase flow simulation-runs results

Porosity	Cell size [m]	Number of cells (Ngb)	$\frac{1}{N_{gb}}$	D [m ² /s]	Interstitial Velocity [m/s]	Flow Rate [m/s]	α [m]	$\frac{\alpha}{cell\ size}$
5 %	0.001	291	0.0034	1.33E-08	1.667E-05	8.34E-07	0.0008	0.80
	0.003	97	0.0103	3.00E-08	1.667E-05	8.34E-07	0.0018	0.60
	0.0049	60	0.0167	4.55E-08	1.670E-05	8.34E-07	0.0027	0.56
	0.0291	10	0.1000	2.52E-07	1.670E-05	8.34E-07	0.0151	0.52
10 %	0.001	291	0.0034	5.40E-09	8.312E-06	8.34E-07	0.0006	0.65
	0.003	97	0.0103	1.37E-08	8.333E-06	8.34E-07	0.0016	0.55
	0.0049	60	0.0167	2.15E-08	8.351E-06	8.34E-07	0.0026	0.53
	0.0291	10	0.1000	1.25E-07	8.351E-06	8.34E-07	0.0149	0.51
22 %	0.001	291	0.0034	2.00E-09	3.786E-06	8.34E-07	0.0005	0.53
	0.003	97	0.0103	6.00E-09	3.789E-06	8.34E-07	0.0016	0.53
	0.0049	60	0.0167	9.50E-09	3.786E-06	8.34E-07	0.0025	0.52
	0.0291	10	0.1000	5.66E-08	3.903E-06	8.34E-07	0.0145	0.50
40 %	0.001	291	0.0034	1.10E-09	2.077E-06	8.34E-07	0.0005	0.53
	0.003	97	0.0103	3.20E-09	2.082E-06	8.34E-07	0.0015	0.51
	0.0049	60	0.0167	5.10E-09	2.087E-06	8.34E-07	0.0024	0.50
	0.0291	10	0.1000	3.09E-08	2.146E-06	8.34E-07	0.0144	0.49

An interesting observation for dispersivity was the fact of its value being often equal to half of the grid block size (column $\alpha/cell\ size$ in Table 1). The reason for the dispersivity increase in the 5% porosity case for 0.001-0.003 m cell size in x-direction most probably the result of the wrong time step. As the available volume for the flow is smaller than in the rest of the cases,

the flow velocity is higher (the injection rate was kept constant for all the cases mentioned in the table), consequently, a smaller time step should be chosen for calculations.

The simulations prove the correlation shown by Herzer and Kinzelbach (1989), Notodarmojo et al. (1991) and Willemsem (1992) for numerical dispersivity for the case of no chemical reaction present (Δx stands for cell size):

$$dispersivity = \frac{\Delta x}{2} \quad (3.1.12)$$

As we know, one of the techniques to reduce numerical dispersion is to reduce the grid block size almost to infinitely small size. Obviously, that is impossible to do in a simulation but it is still possible to run a set of simulation and linearly extrapolate the results to infinitely small grid-block size.

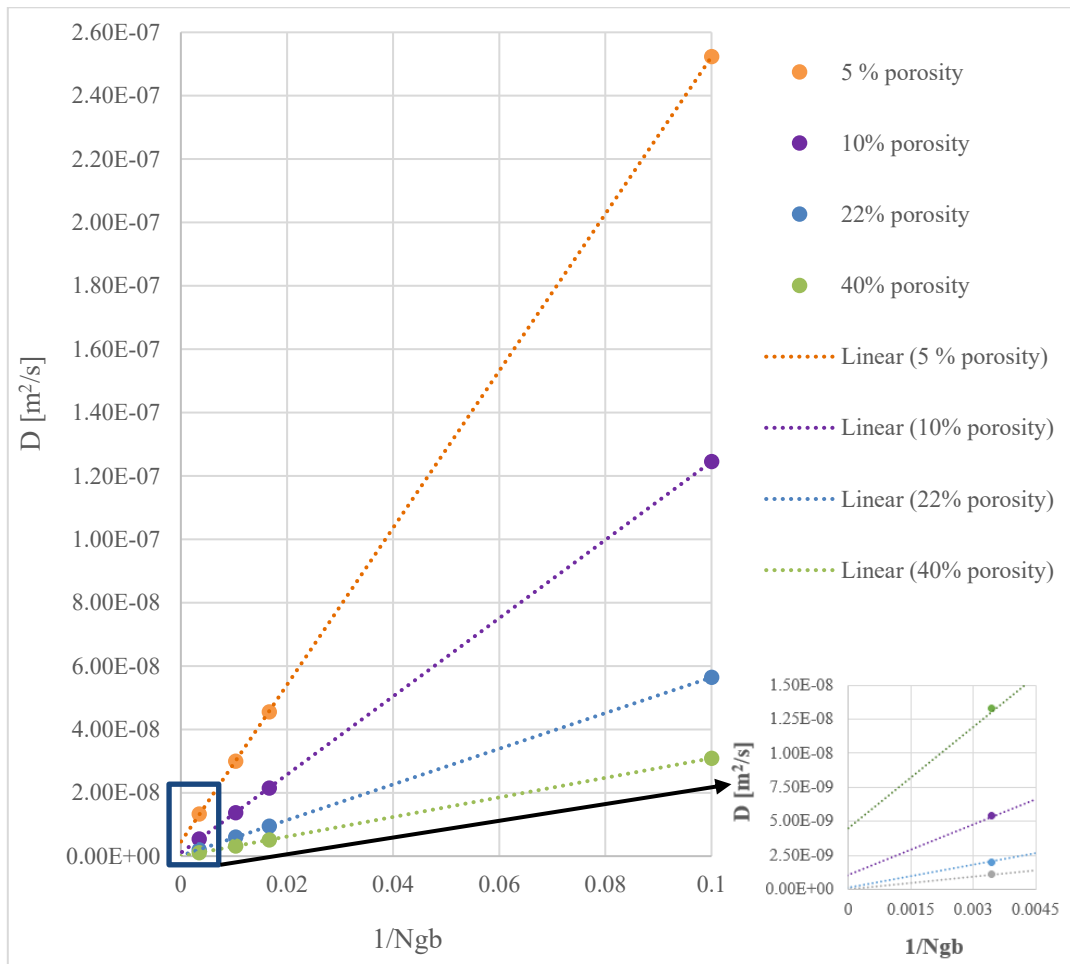


Figure 7. Dispersion versus reverse number of grid blocks. Ngb stands for number of grid blocks.

Figure 7 gives the correlation of longitudinal dispersion with the reverse number of grid blocks ($\frac{1}{N_{gb}}$) and porosity. The smaller the grid-block size, the bigger the number of grid-blocks required to set-up the model. An infinite number of grid-blocks would mean that $\frac{1}{N_{gb}} \rightarrow 0$.

From Figure 7 it is clear that the extrapolated dispersion is not equal to zero, though it is very small compared to what we will see in the heterogeneous case. Depending on the porosity value it varies from $2 \cdot 10^{-12}$ to $5 \cdot 10^{-9}$ meters.

The comparison of dispersion and dispersivity plots makes it clear that porosity influences on the tracer flow velocity. The different slopes for different porosity values that we observe in Figure 7 are no longer present in Figure 8.

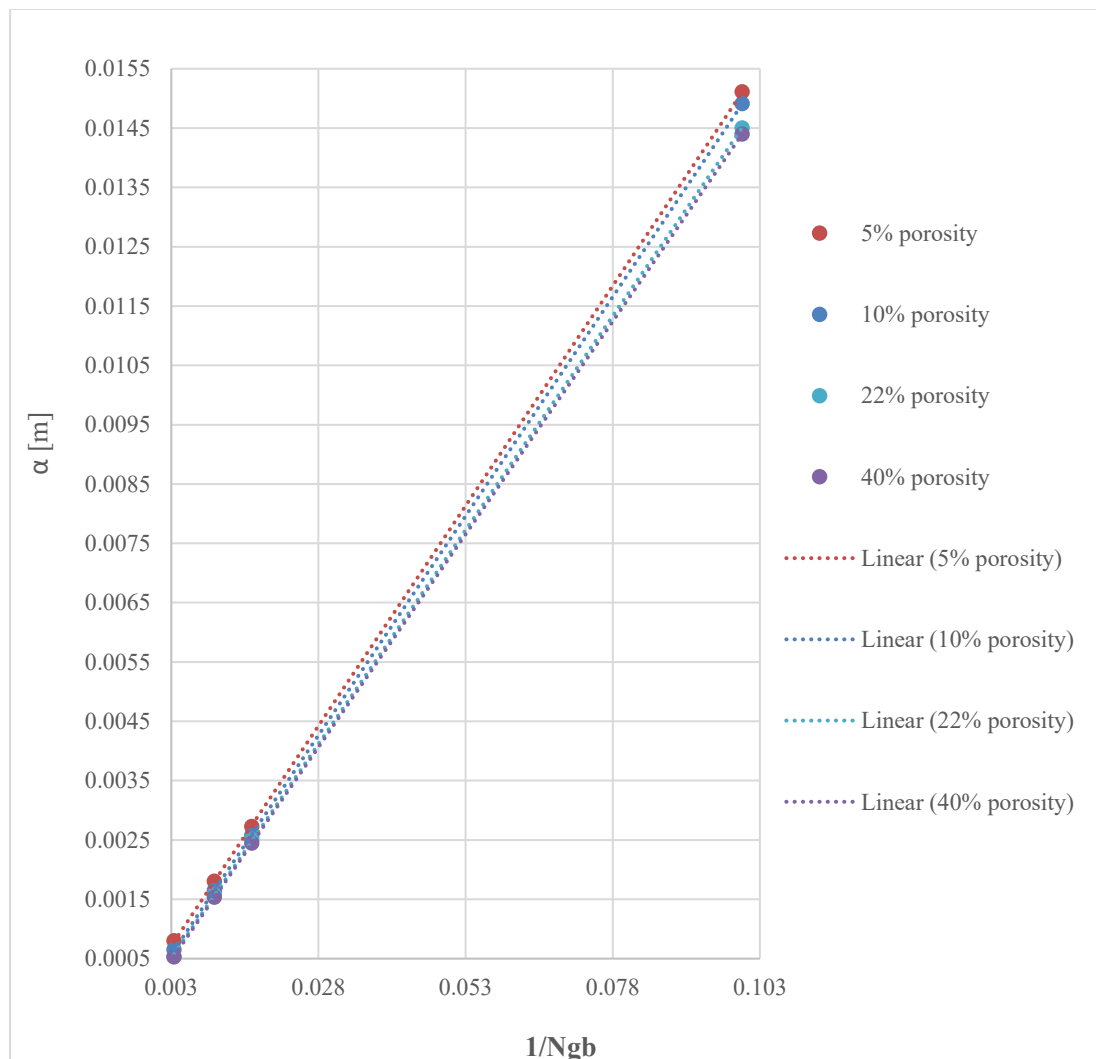


Figure 8. Dispersivity versus reverse number of grid blocks. N_{gb} stands for number of grid blocks

The conclusion from the data displayed in Figure 3 and Table 1, and Herzer and Kinzelbach (1989) correlation is that dispersivity is a property depending mainly the grid-block length in

single-phase flow homogeneous model simulations when the calculation time-step size is chosen carefully.

When the porosity of the system is changed, there is less volume available for the flow, therefore water travels faster when the input injection rate is not changed with the change of input porosity value. The correlation of the interstitial velocity with porosity is displayed in Figure 9 and Figure 10.

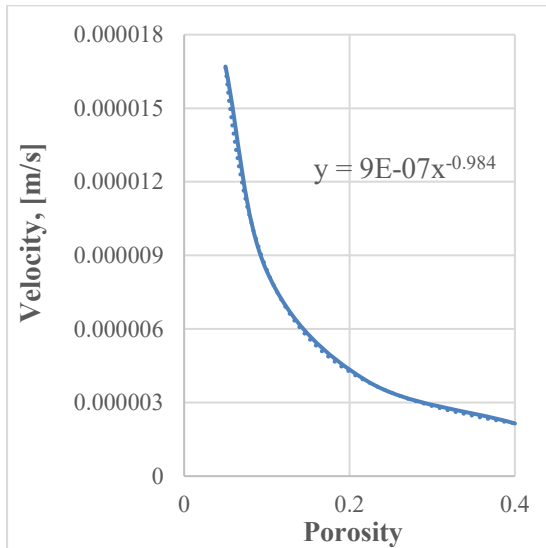


Figure 9. Velocity correlation with porosity

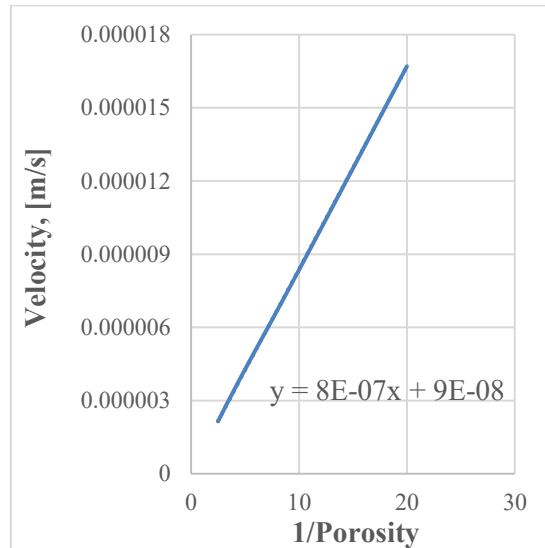


Figure 10. Velocity correlation with the reverse value for porosity

Further, the core-scale model was increased to a 150 m model, preserving the other settings as they were and changing only the size, time step and injection rate. This experiment proved that we get the same value for dispersivity (half-cell length) as for core-scale.

3.2 Multi-phase (oil and water) flow

Correlation 3.1.12 was proven for a single-phase homogeneous flow in a 150 m model; oil was introduced as a second phase of the simulated model. Relative permeability functions are available in Figure 11; the values are given in Table 2.

The model set-up also required a small alteration of the water properties:

- 100 bar reference pressure
- 0.47 cP viscosity
- 1.0061 formation volume factor
- 1000 kg/m³ density at surface conditions

The introduced oil was of the “dead” type, with no dissolved gas. Further, in the field-scale heterogeneous case, work was done only with dead oil, as gas would have brought a severe impact on our results with a minor contribution to the topic of the research. The properties of the oil were the following ones:

- 100 bar reference pressure
- 3.8 cP viscosity
- 1.1 formation volume factor
- 905 kg/m³ density at surface conditions
- 0.05 kg/m³ density of the solute gas at surface conditions

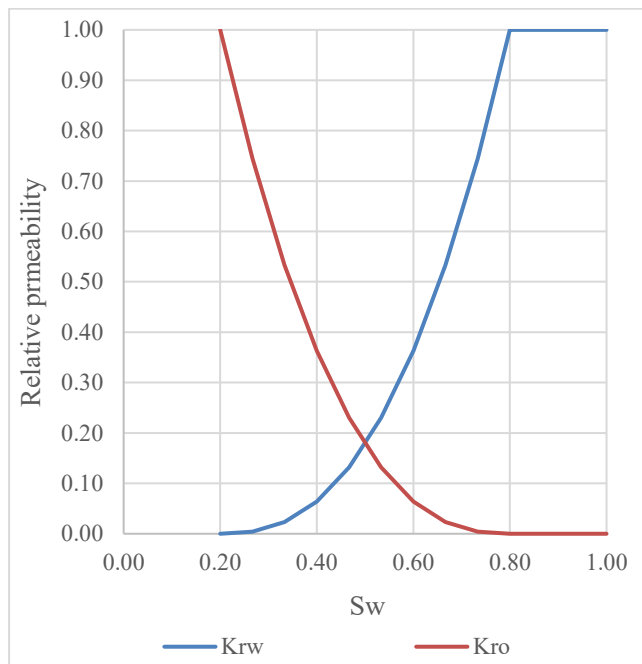


Table 2. Relative permeability input

Sw	Krw	Kro
0.200	0.000	1.000
0.267	0.004	0.745
0.333	0.023	0.534
0.400	0.064	0.363
0.467	0.132	0.230
0.533	0.230	0.132
0.600	0.363	0.064
0.667	0.534	0.023
0.733	0.745	0.004
0.800	1.000	0.000
1.000	1.000	0.000

Figure 11. Relative-permeability functions for the two-phase flow in homogeneous media

Dispersion and dispersivity were observed in correlation with the sample average saturation when half of the tracer concentration is produced. It was done by running the simulation of multiple passive tracers injection. This procedure was done for low viscosity oil, the properties of which were already described, and high viscosity (40 cP) oil. Relative permeability functions used were the same for both cases.

The simulations were run until the models almost reached residual oil saturation state, where almost only water and tracer flow was present. This was done to prove that even for initially two-phase saturation case the dispersivity for the residual-oil saturation-state is close to the relation described in equation 3.1.12 ($\Delta x = 1\text{m}$). It means that for the systems with no movable-

oil the linear correlation of dispersion with the reverse number of grid-blocks is valid (Figure 7 and Figure 8).

High oil viscosity case showed lower dispersion and dispersivity values than the low viscosity case (Figure 12 and Figure 13), though the shapes of correlation-trends were highly alike:

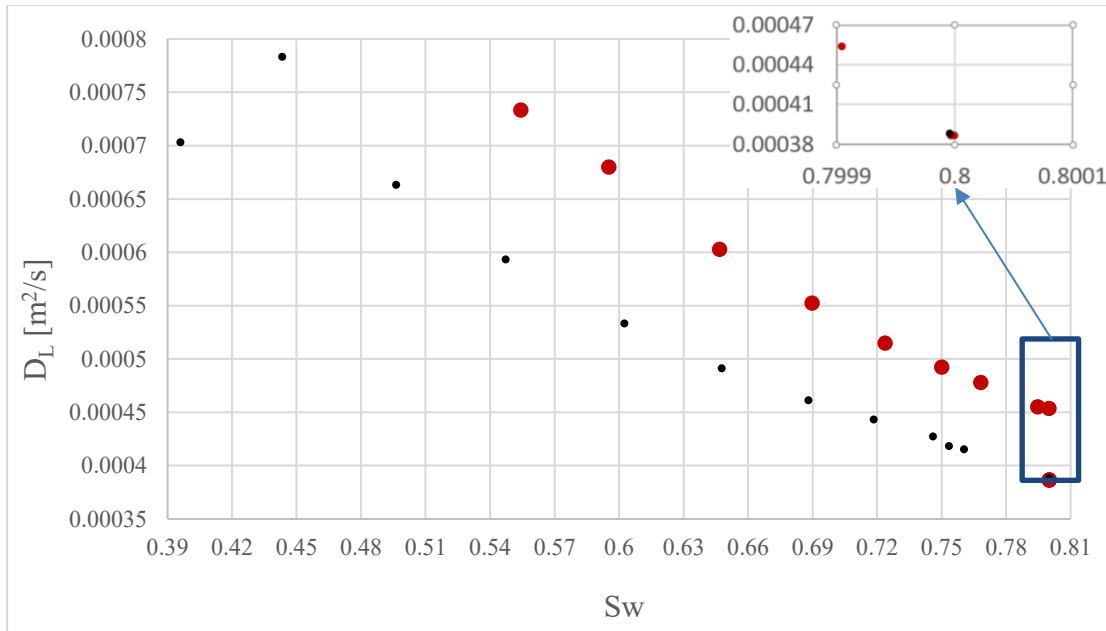


Figure 12. Dispersion versus sample average water saturation.

Red circles for low viscosity oil (3.8 cP), black circles for high viscosity oil (40 cP).

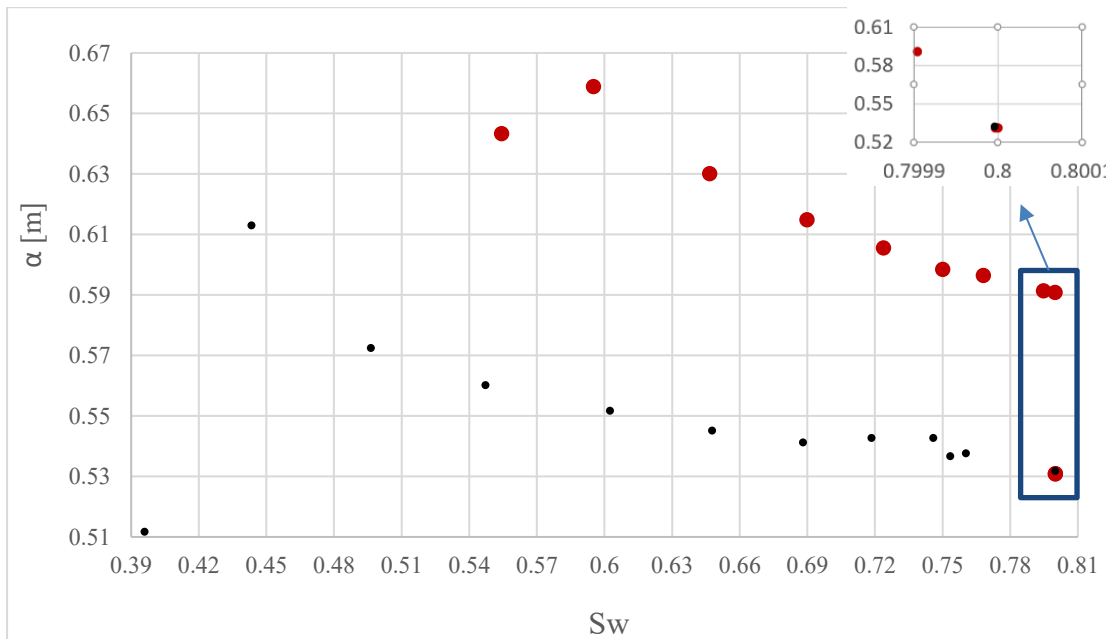


Figure 13. Dispersivity versus sample average water saturation.

Red circles for low viscosity oil (3.8 cP), black circles for high viscosity oil (40 cP).

The first tracer was injected with the start of water injection and the second one was injected shortly after the first one. The second tracer showed an increase in dispersivity in comparison to the first one. The tracers injected after the second one displayed the decrease of dispersion and dispersivity with the core-plug model's average water-saturation increase.

As it gets closer to the oil residual saturation the dispersion and dispersivity decrease is very rapid in for the lower oil-viscosity case. The interstitial velocity decrease is also rapid in this case (Figure 14).

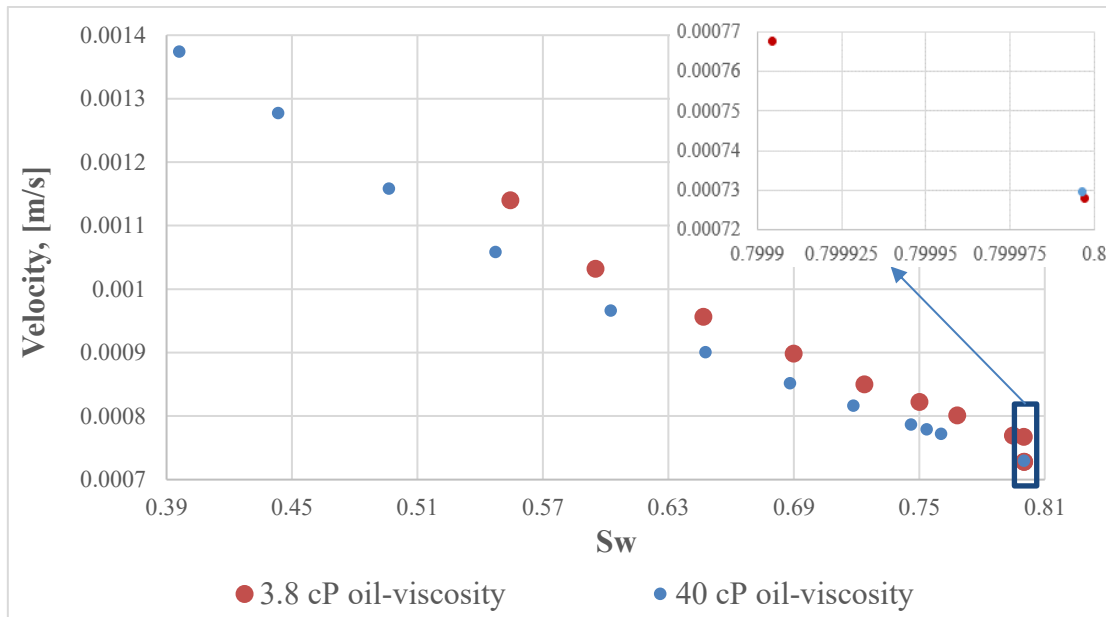


Figure 14. Velocity versus sample average water-saturation

Water velocity decrease with the increase of core-plug average water-saturation is displayed in Figure 14. The more oil is displaced from the core, the more volume is available for the flow of water-phase, therefore the velocity decrease is observed.

3.2.1 Chemical relative permeability model in Eclipse

Injection of alkali is creating in-situ surfactant in the reservoir. Therefore, in the simulation program code, keywords for surfactant and polymer are used to simulate alkaline-polymer flooding.

The input concentration of the injected chemicals in the injected water was the following:

- Polymer: 2 kg/m³
- Surfactant: 7 kg/m³

Further, chemical distribution is modeled by the conservation equation within the water phase. The concentration is calculated at the end of each time-step using the fully implicit method after the calculations of water and oil is done.

The eclipse model for surfactant relative permeability is making the transition between low capillary numbers (immiscible relative permeability curves) to high capillary numbers (near miscible relative permeability curves).

The capillary number (N_c) is a dimensionless ratio of viscous forces to capillary forces:

$$N_c = C_N \frac{\|K \cdot \nabla P_o\|}{\sigma_{ow}} \quad (3.2.1.13)$$

Where

K = permeability,

∇P_o = gradient of the potential,

σ_{ow} = interfacial tension,

C_N = conversion factor (depends on the units used).

The input of data for interfacial tension in Eclipse is done using the SURFST keyword. The input for the investigation was the following one:

```

SURFST
-- Concentration, [kg/m3]  Tension, [N/m]
      0                      0.03
      7                      0.0013/

```

Where concentration stands for the surfactant concentration in the injected water phase and tension stands for interfacial tension (σ_{ow}). This data is later linearly interpolated by Eclipse. For each surfactant-concentration capillary number is calculated.

To use the surfactant model in Eclipse, the TABDIMS keyword is modified as it is necessary to add relative-permeability function for a miscible flood. That requires to change the first value of the keyword from 1 to 2, meaning the number of saturation tables entered will now be 2.

Saturation function region numbers are entered in the SATNUM keyword. This action specifies the set of saturation functions that will be used for relative-permeabilities and capillary pressures calculations in each grid block.

The data for the linear correlation of miscible flow oil relative-permeability versus saturation is added in the SOF2 keyword; SWFN keyword is used for water case the:

```

SOF2                               SWFN
--Kro      So                      --Krw      Sw
0.05       0                       0.2        0
0.8        1/                      0.95

```

The immiscible relative-permeability functions were not changed from the ones already displayed. Miscible and immiscible curves will be scaled based on the capillary number, which changes with the change of surfactant concentration.

The interpolation parameter F_{kr} is given in the SURFCAPD keyword as a tabulated function of the $\log_{10}(N_c)$, so that the weighting factor F is:

$$F = F_{kr}(\log_{10}N_c) \quad (3.2.1.14)$$

SURFCAPD

$-\log_{10} N_c$	<i>miscibility</i>	
-10	0	} Immiscible
-5.725	0	
-2.649	1	} Miscible
2	1/	

In other words, when $\log_{10} N_c$ is within the range of -10 to -5.725, F is equal to 0, and the simulator uses the initial relative-permeability curves for immiscible flow. When $\log_{10} N_c$ is within the range of -2.649 to 2, F is equal to 1 and the simulator uses the initial relative-permeability curves for near miscible flow.

However, if $\log_{10} N_c$ is between -5.725 and -2.649, the relative permeability curves have to be adjusted to account for the partially miscible flow conditions, using the following steps:

1. The value of F for $\log_{10} N_c$ is linearly interpolated between (-5.725, 0) and (-2.649, 1)

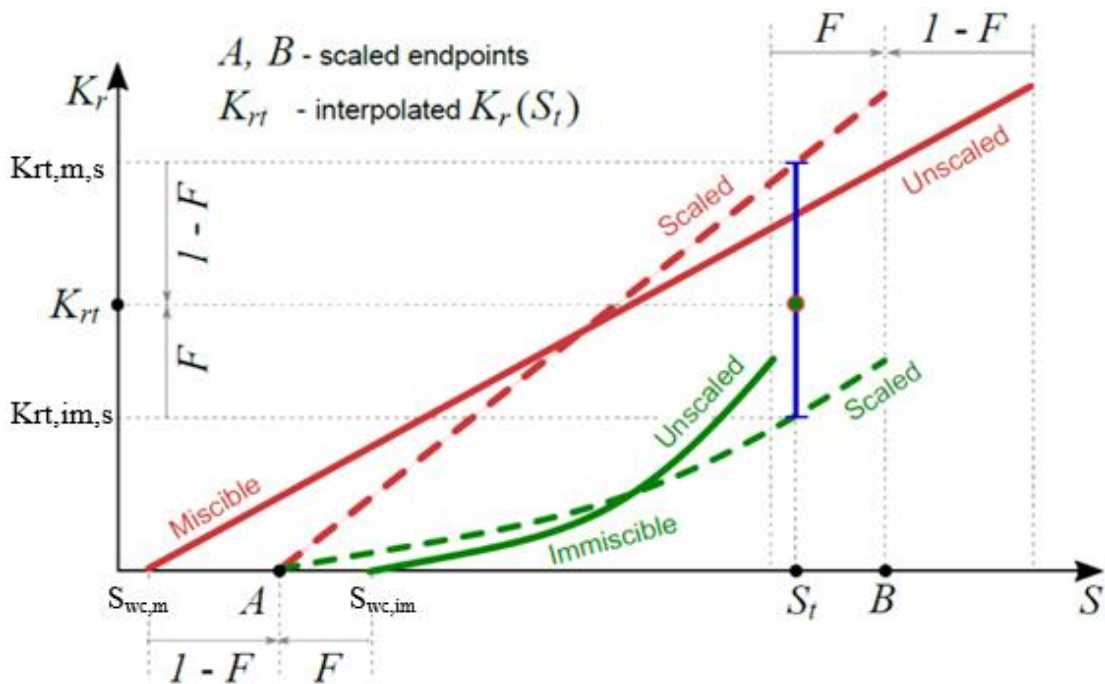


Figure 15. Calculation of the relative permeability, Eclipse manual

2. The miscible and immiscible curves are scaled as shown in Figure 15, by interpolating the saturation endpoints of both the miscible and immiscible curves. To reach the scaled endpoint saturation A , the miscible connate water saturation is shifted to the right by:

$$A = S_{wc,m} + (S_{wc,im} - S_{wc,m}) \cdot (1 - F) \quad (3.2.1.15)$$

and the immiscible connate water saturation is shifted to the left by:

$$A = S_{wc,im} - (S_{wc,im} - S_{wc,m}) \cdot F \quad (3.2.1.16)$$

To reach the endpoint saturation B , the residual saturations are scaled in a similar manner, but with the weighting factors and directions reversed.

3. For a grid block saturation S_t , the interpolated relative permeability value K_{rt} is calculated by interpolating between the scaled relative permeability curves, and their values $K_{rt,m,s}$ and $K_{rt,im,s}$:

$$K_{rt} = K_{rt,im,s} + (K_{rt,m,s} - K_{rt,im,s}) \cdot F \quad (3.2.1.17)$$

3.2.2 Alkali-polymer in oil/water flow for 1D homogeneous case

After the model reached residual oil-saturation, further injection of water only will not bring any incremental oil recovery. Thus, chemicals should be injected to continue oil production. Here, alkaline-polymer flood with multiple tracer injection is simulated. The first tracer injection starts together with an alkaline-polymer flood and continues until the end of the simulation. Alkaline-polymer injection ends once the desired volume of AP has been injected. The injection of the second tracer starts ten days after the stop of alkaline-polymer injection and lasts also for 10 days. At this point, the simulation stops.

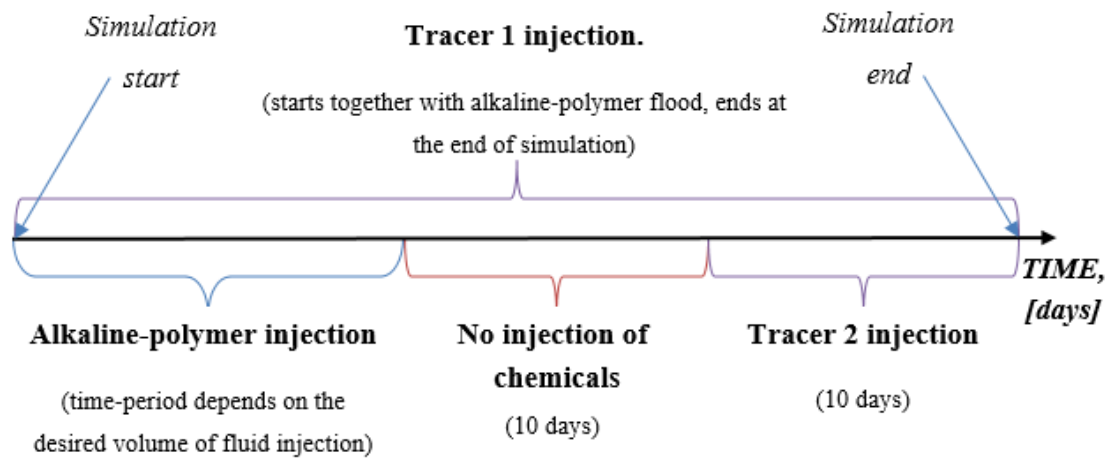


Figure 16. Injection schedule

Tracer injection in all cases in continuous and stops only with the end of the simulation. Therefore for each simulation, the injection time for the first tracer was different, depending on the volume of alkaline-polymer injection. The point in time when the cumulative produced tracer volume was equal to half of the injected tracer volume therefore also depended on the volume of alkaline-polymer injected. So, the saturation-state of the simulated model, when tracer 1 production value is equal to half of the cumulative amount of the injected tracer 1, is different for each simulation.

This is done to see the change of dispersion and dispersivity for the case when oil viscosity is equal to 3.8 cP. The first tracer showed no dispersion and dispersivity change with the change of saturation (Figure 17 and Figure 18). However, when the system is close to the state of no movable oil left, dispersivity turned to be half of the grid-block length.

At the start of the alkaline-polymer injection, oil is mobilized. Therefore, the simulated model is a two-phase flow system. Dispersion and dispersivity of a two-phase flow system are higher than of a single-phase flow system, as it was already shown in previous examples. Near the state of no movable oil left, dispersion has a rapid decrease

In Figure 17 and Figure 18, pV stands for pore volume and AP stands for alkaline-polymer.

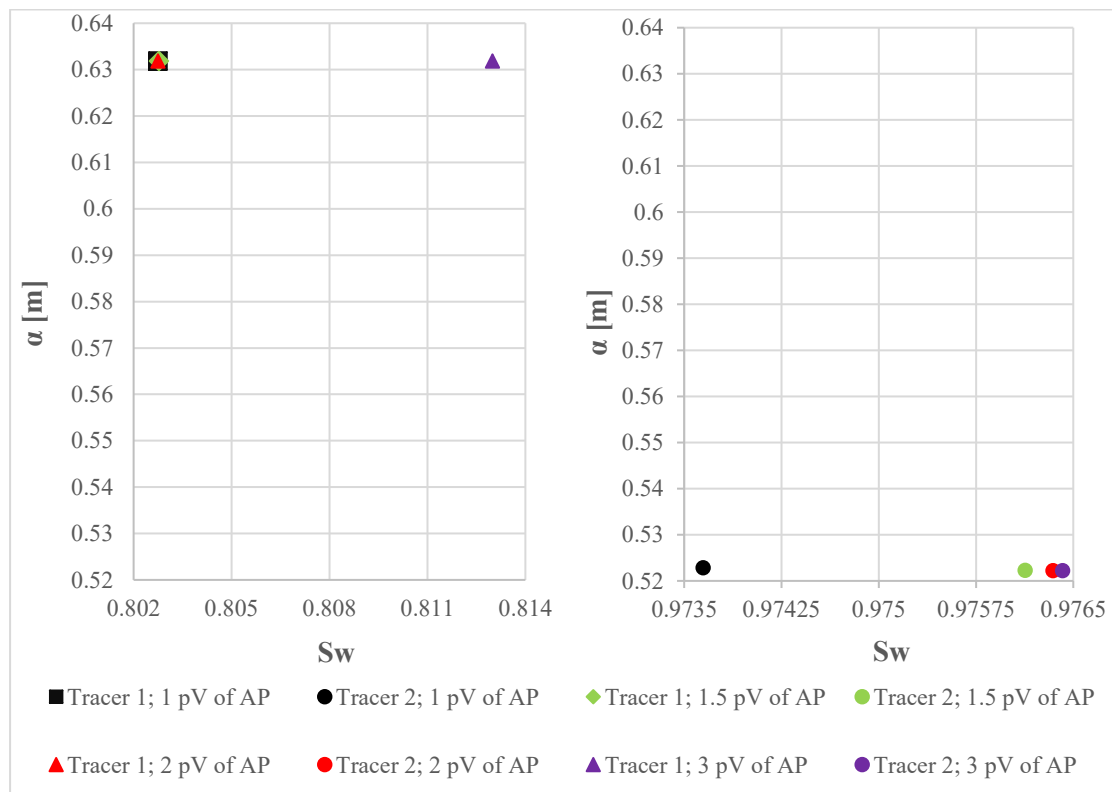


Figure 17. Dispersivity versus sample average water saturation while alkaline-polymer flood

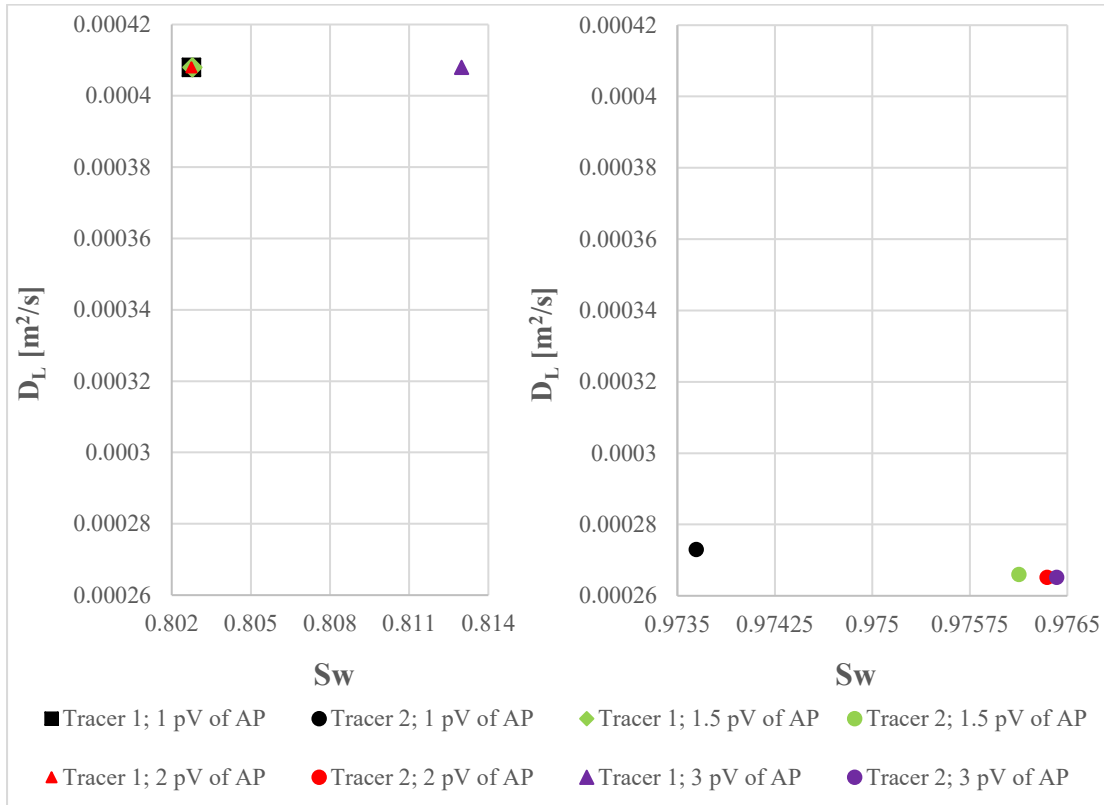


Figure 18. Dispersion versus sample average water saturation while alkaline-polymer flood

Chapter 4 2D model

2D permeable media model for the flow simulation was built based on data from the Matzen field, 16 Tortonian Horizon reservoir. This field already had a successful polymer flooding project that proved the concept of EOR in the field, therefore, it is now planned to perform an alkaline-polymer flooding project in the reservoir. A geological model based on SP-logs (spontaneous potential) from wells BO-157 and BO-81 was constructed by John Nejedlik, MSc (Reservoir Geoscience). The interpretation of Porosity from the SP logs was calibrated with all available core data from across the field (see Figure 19).

These two wells were chosen as they fulfilled the following criteria:

- ~ 165 m distance between the wells (150 m is the typical well spacing in the reservoir, and this makes the study guided by the real field example)
- ~ Equal reservoir thickness in both wells (~25m)
- ~ Minimal angle of the dipping of the reservoir

This distance was chosen to be able to run simulations on three different scales (55m, 110m, and 165m) to understand the correlation between dispersion and dispersivity with distance. There are areas within the field where the reservoir thickness varies, however equal thickness (~ 25m) is important in this study to avoid any impact on flow due to thickening or thinning of the reservoir.

For the homogeneous case, the porosity and permeability were set to the mean value of the heterogeneous case. A detailed description of the introduced heterogeneity is given in the next section together with a brief geological background of the reservoir.

4.1 Geological background and heterogeneity distribution

The Matzen 16.TH reservoir is an approximately 25 m thick sandstone with reservoir properties typically ranging between 100 mD to 1 D (see Figure 19). The reservoir was deposited as laterally extensive sand-rich deposits reworked in a marginal marine environment within distinct transgressive successions. In the report for OMV by Proseis AG (2003), it is stated that the sands are sheet-like and unconfined and show excellent connectivity.

Figure 19. Permeability versus porosity functions. Grey line for silty shale, yellow line for fine sand, orange line for coarse sand.

Core-data was used to identify three Flow Zone Indicator (FZI) “rock types”. These rock types were interpreted at the wells and Porosity distributed in the model by rock type. Each rock type was then assigned a separate permeability function (Figure 19) which provided the mechanism for introducing heterogeneity into the models.

The log character is often described as “blocky” (see Figure 20) because the interpreted Vsh log shows little variability, suggesting a relatively homogeneous reservoir. Heterogeneity clearly exists but may be somewhat masked by the low vertical resolution (1-3meters) of the existing Spontaneous Potential (SP) logs.

The rock type distribution between the wells is displayed in Figure 20. Monitoring well 1 and Monitoring Well 2 are the wells that do not exist physically and are only used in the simulations to monitor dispersion between the real wells.

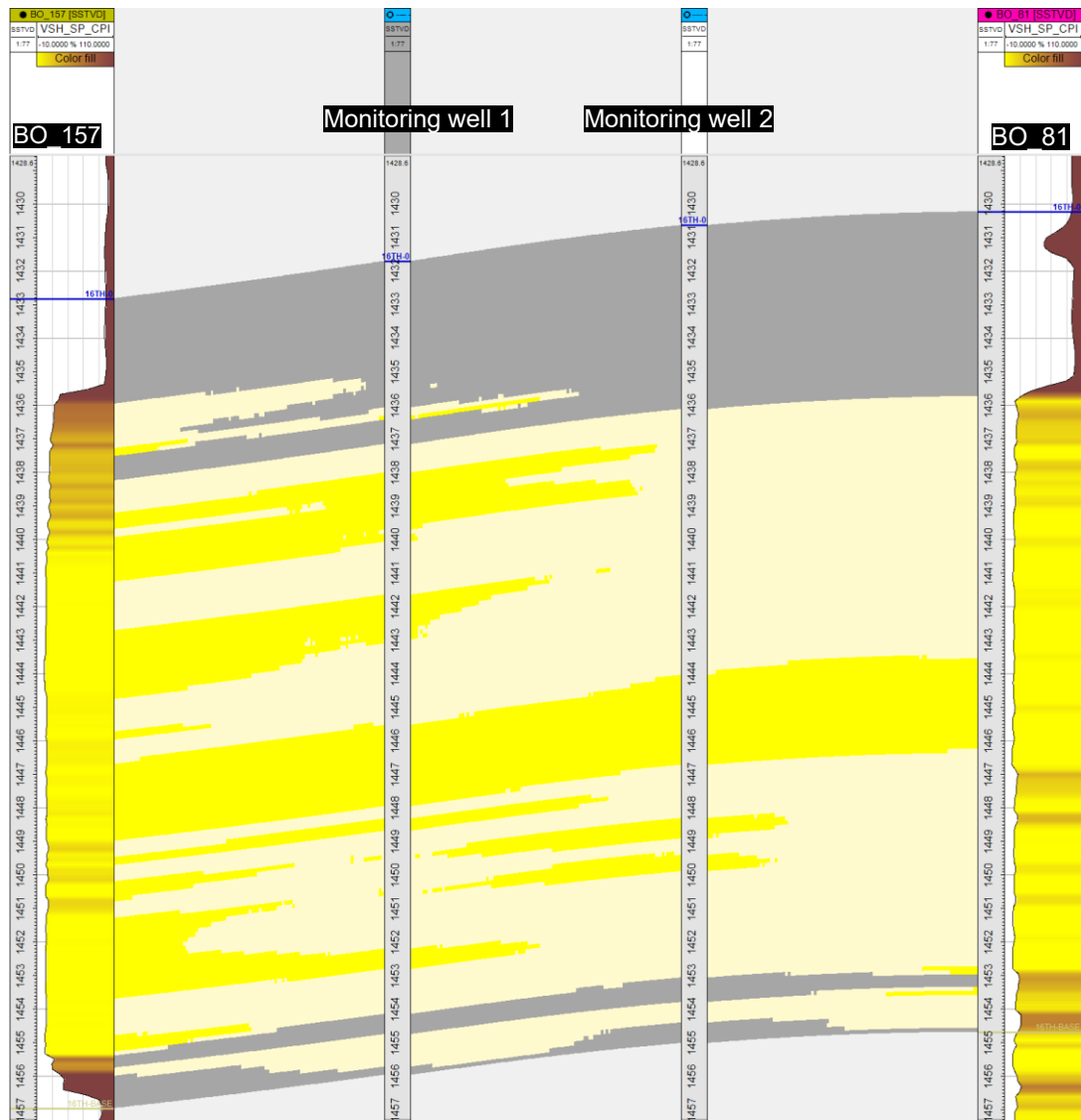


Figure 20. Interpolated Rock-type distribution between BO_157 and BO_81 (location of monitoring wells are shown for reference)

Rock type and porosity were upscaled (blocked) for the two wells and data analysis performed. This analysis observed the proportion of the three rock types in each layer in the model (see Figure 21), and defined the porosity distributions for each rock type. Given only two real wells were used in this study, the proportions of any rock type observed in a layer at one of the wells but not observed in the same layer of the second well is shown to have a proportion of 50%. A typical data analysis uses all available wells within the field therefore the proportions of rock type observed in each layer would normally vary much more significantly.

Truncated Gaussian simulation (TGS) was used to interpolate the rock data between the wells. A single variogram was used to control how far between the wells each rock type was distributed. For the purpose of this study, the variogram range was arbitrarily set to 100 meters, or less than the distance between the wells with an azimuth aligned with the orientation between

the wells (60deg). The TGS algorithm honours the well data and ultimately controls how close the rock types from BO_157 are modelled toward BO_81, and vice versa. Put simply, were the variogram range made smaller, the coarse sands (bright yellows) observed in well BO_157 would not extend as far toward the well BO_81 (where they are not observed).

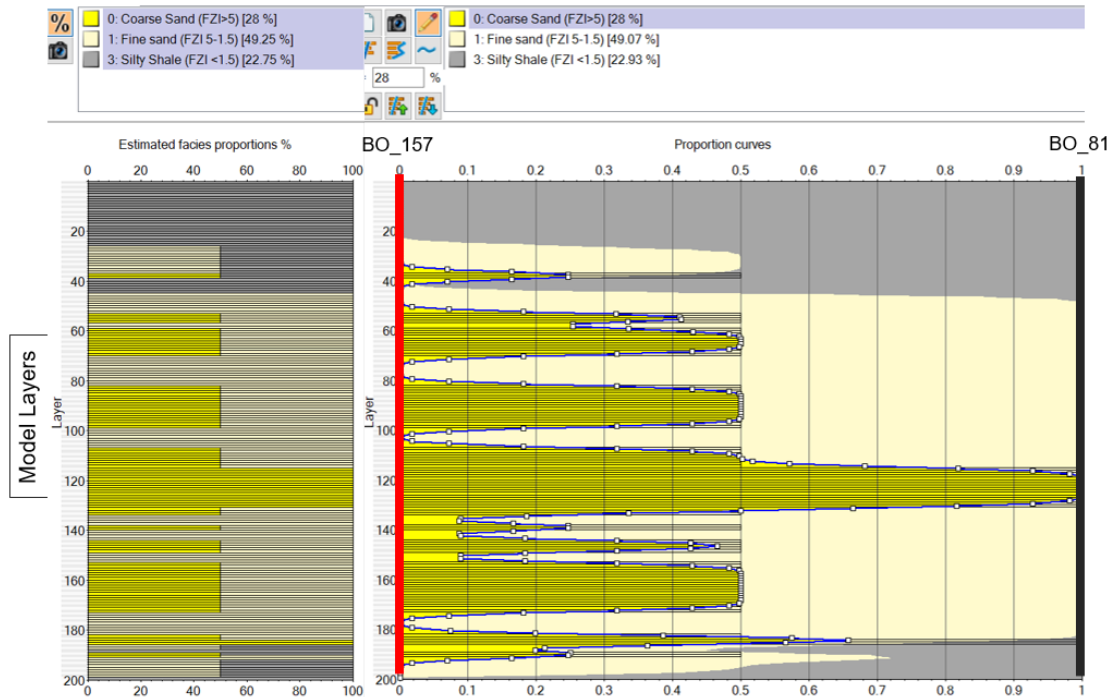


Figure 21. Data analysis for facies

Porosity modeling was done using the Gaussian random function algorithm. Distribution of porosity for each of the three rock types was established in the data analysis which was in-line with the distributions observed from across the field. Silty shale has a mean porosity of 13%, Fine Sand 27%, and Coarse sand has a mean of 29%. The properties for porosity were then distributed according to the three rock types using the same variogram as the rock type modelling. The difference between the coarse and fine sand is not too large, and this can be seen in Figure 22 which shows subtle distinction between the coarse and fine sand, however, however the difference becomes apparent once the different permeability functions are applied to the porosity (Figure 23).

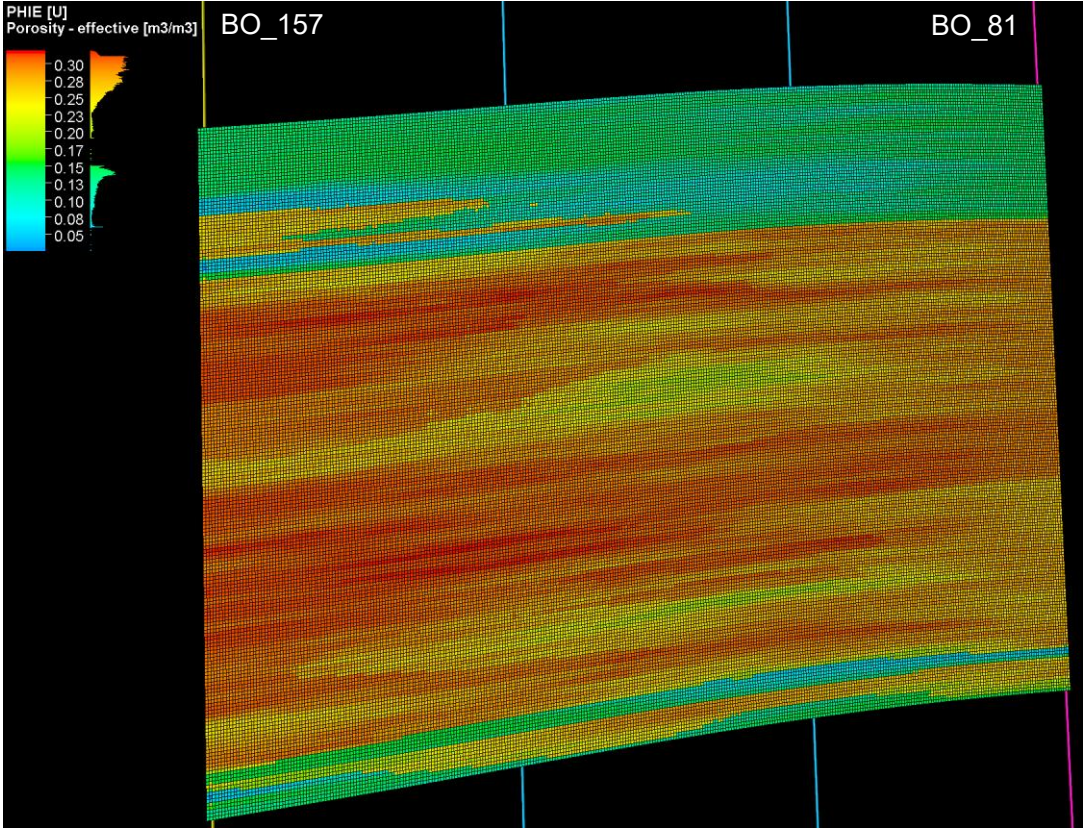


Figure 22. Fine-model porosity distribution

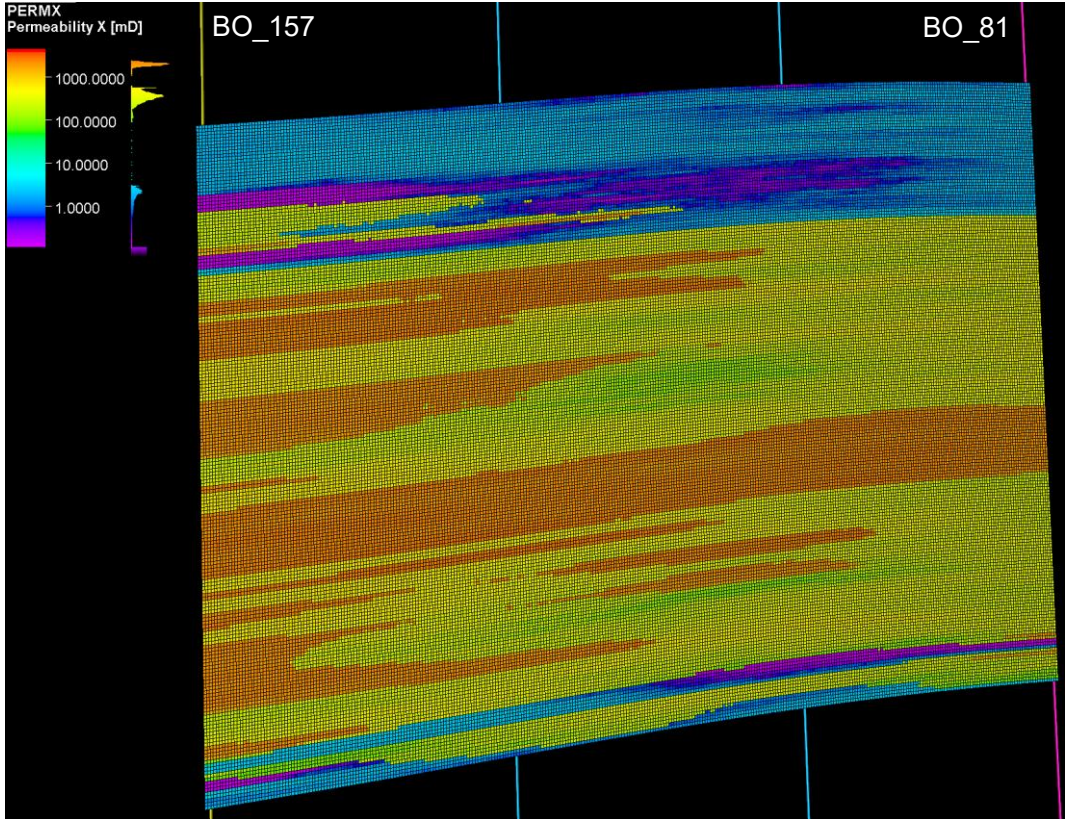


Figure 23. Fine-model permeability distribution

The next step was creating models with bigger grid sizes from which the properties of the fine scale model would then be upscaled to. The different properties were then upscaled using different approaches. Rock types were upscaled by taking the “most of” approach whereby the discrete rock type which intersects most of the cell is selected. Porosity was upscaled by performing arithmetic volume-weighted averaging, while permeability upscaling was flow-based with no-flow boundaries, using a finite-difference algorithm.

Figure 24 and Figure 25 display the result of the permeability upscaling in x-direction, for two gridding examples:

- 5 m in x-direction and 0.25 m in z-direction
- 10 m in x-direction and 0.5 m in z-direction

As it was already stated, grid-upscaling reduces the heterogeneity of the simulated model and that is clearly visible from the two examples below, especial in comparison with the model with the original, fine grid.

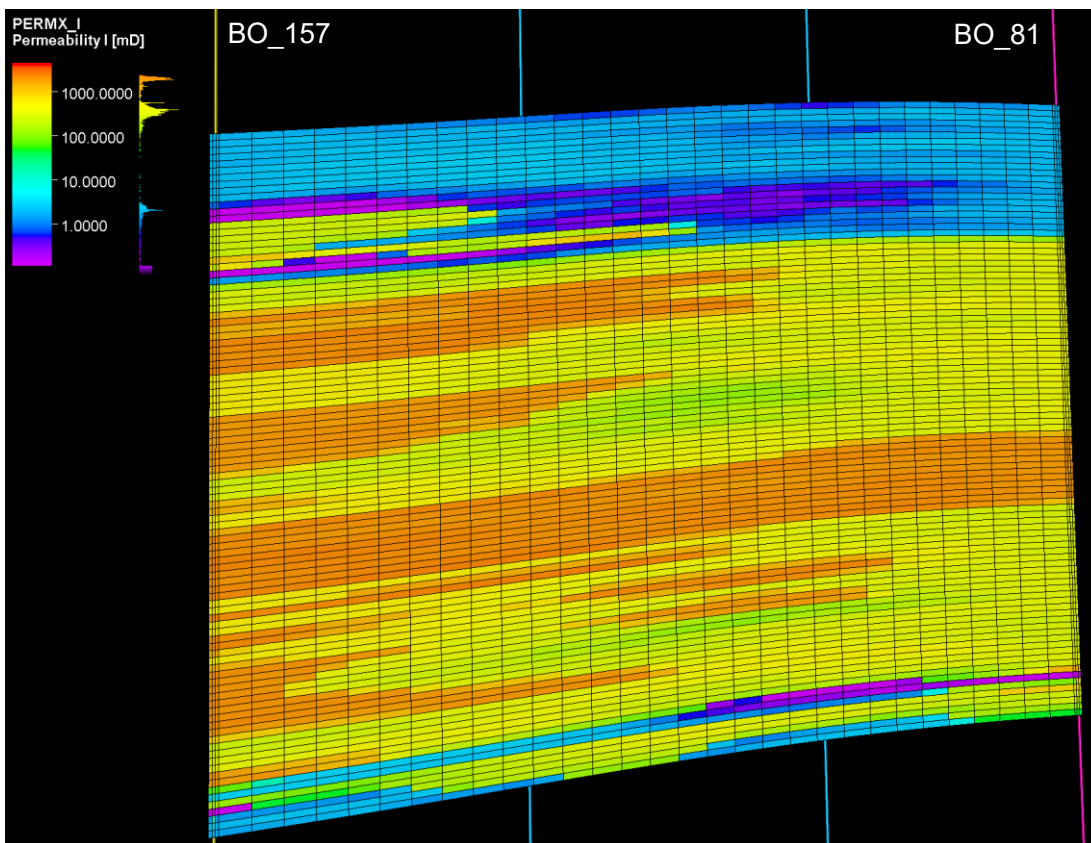


Figure 24. Permeability distribution for gridding size: 5 m in x-direction and 0.25 m in z-direction

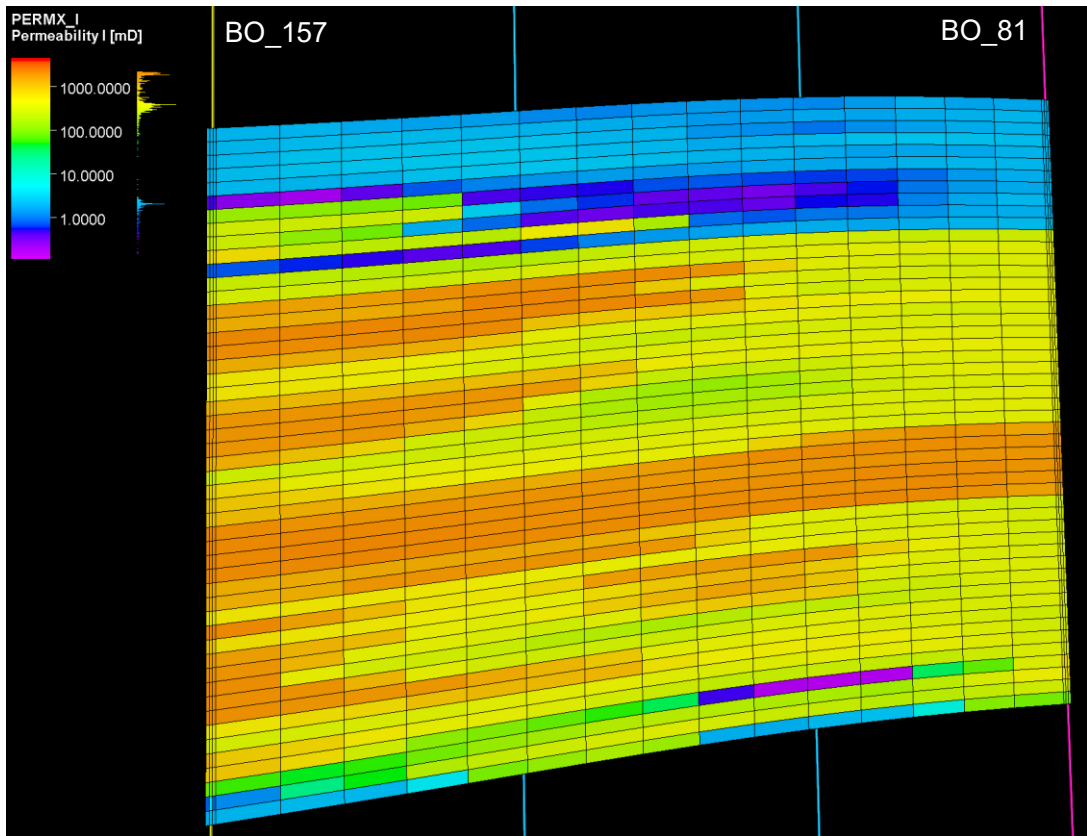


Figure 25. Permeability distribution for gridding size: 10 m in x-direction and 0.5 m in z-direction

4.1.1 Permeability upscaling

Here is the algorithm of how Petrel treats flow-based permeability upscaling with no-flow boundaries:

1. Set of fine cell corresponding to the coarse target cell is determined.
2. Constant pressure drop is maintained on two sides of the coarse cell (Figure 26).

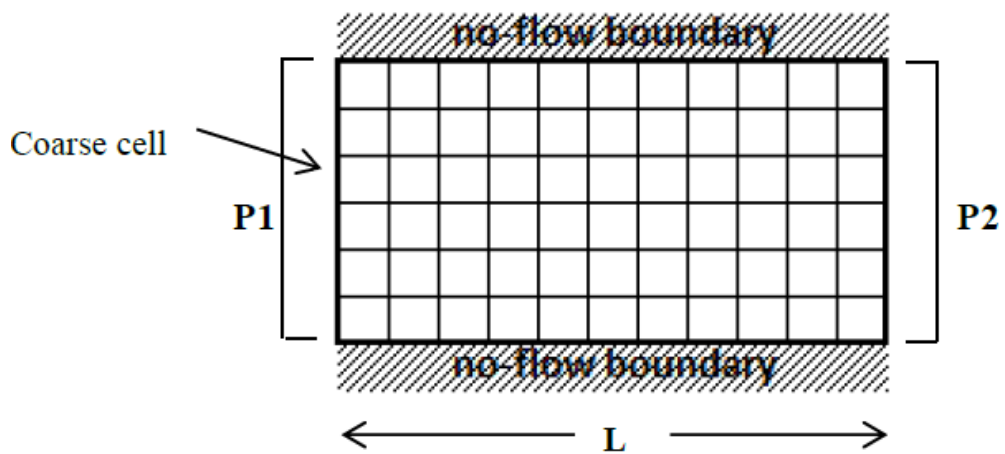


Figure 26. No-flow boundary condition for coarse cell, Fouda (2016)

3. Pressure equation (4.1.18) is solved for each fine grid block that is included within the coarse block:

$$\frac{\partial}{\partial t}(\rho\varphi) - \nabla \cdot \left(\frac{\rho}{\mu} k \cdot \nabla p \right) + \tilde{m} = 0 \quad (4.1.18)$$

Where

φ = rock porosity,

ρ = fluid density,

∇p = pressure drop between two neighboring blocks,

\tilde{m} = source/sink term,

μ = fluid viscosity,

k = permeability.

As the upscaling is done for a static geological model, there are no injection or production wells in the grid-blocks ($\tilde{m} = 0$). Assuming the properties of the model do not change with time $\frac{\partial}{\partial t}(\rho\varphi) = 0$, and $\frac{\rho}{\mu} = \text{const}$ as Petrel is neglecting gravity and viscosity.

Therefore, in steady state, the pressure should satisfy:

$$\nabla(k\nabla p) = 0 \quad (4.1.19)$$

4. The flux, for a fine cell, is given by the product of velocity and porosity, which are constant over a cell:

$$\text{Flux} = \int_V k \cdot \nabla p \cdot \varphi dV \quad (4.1.20)$$

Where V = volume of a fine cell and φ = porosity of a fine cell.

5. The flux through the coarse cell and the sum of fine cells, which are comprised by the coarse cell, shall be identical which results in equation (4.1.21). The coarse cell permeability is derived from this equation:

$$\Phi \cdot K \cdot \int_{V_{c.c.}} \nabla p dV = \int_V k \cdot \nabla p \cdot \varphi dV \quad (4.1.21)$$

Where $V_{c.c.}$ = volume of a coarse cell and Φ = porosity of a coarse cell.

4.1.2 Dispersion and dispersivity calculations

The Ogata and Banks (1961) solution for the convection-dispersion equation, that was mentioned in the introduction, for the one-dimensional model has to be modified to be applicable for two-dimensional flow. Escuder et al. (2009) applied another strategy in their book.

The input data for that strategy is the ratio of produced to injected tracer versus time (Figure 27), where the starting point for the time input is the beginning of injection. Two time ranges, σ_{16} and σ_{84} , are highlighted out of the given input: one from the time when the ratio reaches 16% to 50% (σ_{16}), the other from 50% to 84% (σ_{84}).

The nomenclature in Figure 27 is the following: C_0 stands for the cumulative injected tracer concentration; C is the cumulative tracer production. Time axis displays the time since the beginning of the injection; t_0 is the time when half of the injected tracer was produced.

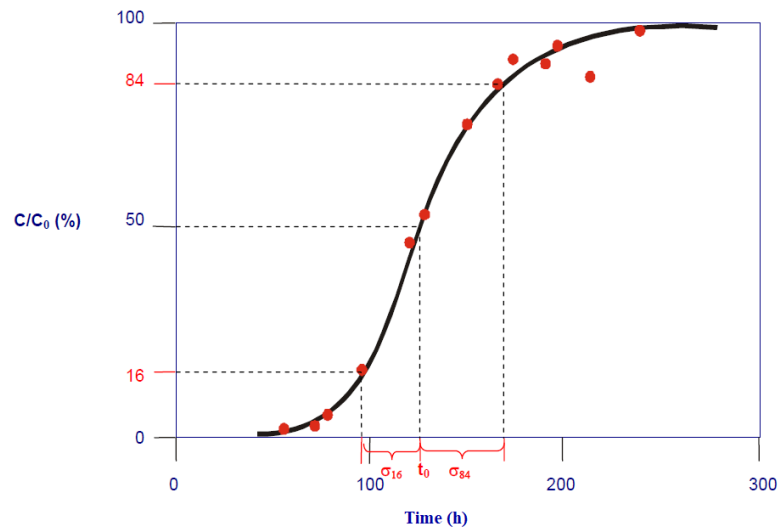


Figure 27. Tracer relative production curve (Escuder et al., 2009).

The equation for the tracer travel velocity is the same as equation (1.1.2).

Equations for dispersion are the following:

$$D_t = \frac{\sigma_t^2 * v^2}{2 * t_0} \quad (4.1.2.22)$$

$$D_{16} = D_{84} = \frac{\sigma_{16}^2 * v^2}{2 * t_0} \quad (4.1.2.23)$$

$$D_{84} = D_{84} = \frac{\sigma_{84}^2 * v^2}{2 * t_0} \quad (4.1.2.24)$$

D_{16} and D_{84} and the solution of equation (2.10) are equal for single-phase flow in one dimension. In the two-dimensional case the C/C_0 curve is no longer symmetrical, thus D_{16} and

D_{84} have different values. Therefore, it was decided to introduce an averaging for D_{16} and D_{84} that was based on arithmetical averaging of σ_{16} and σ_{84} :

$$\sigma_{ave} = \frac{\sqrt{\sigma_{16}^2 + \sigma_{84}^2}}{2} \quad (4.1.2.25)$$

$$D_{ave} = Dave = \frac{\sigma_{ave}^2 * v^2}{2 * t_0} \quad (4.1.2.26)$$

This strategy can be applied for the one-dimensional homogeneous case and the results are equal to the results of Ogata and Banks (1961) solution: $D_{16} = D_{84} = D_L$. However, the solution of Ogata and Banks (1961) is applicable only for homogeneous situations, when the tracer-concentration production curve is symmetrical. In the heterogeneous case, this curve is no longer symmetrical. Therefore, some modifications in the solution must be done based on empirical analysis.

4.1.3 Single-phase flow in homogeneous model, tracer in water

Tracer-slug simulation was performed to investigate the flow in the two-dimensional model.

Time step size in this situation is still having a severe impact on the numerical dispersion and that makes it important to choose the right time-step size to make an adequate comparison of models of different sizes.

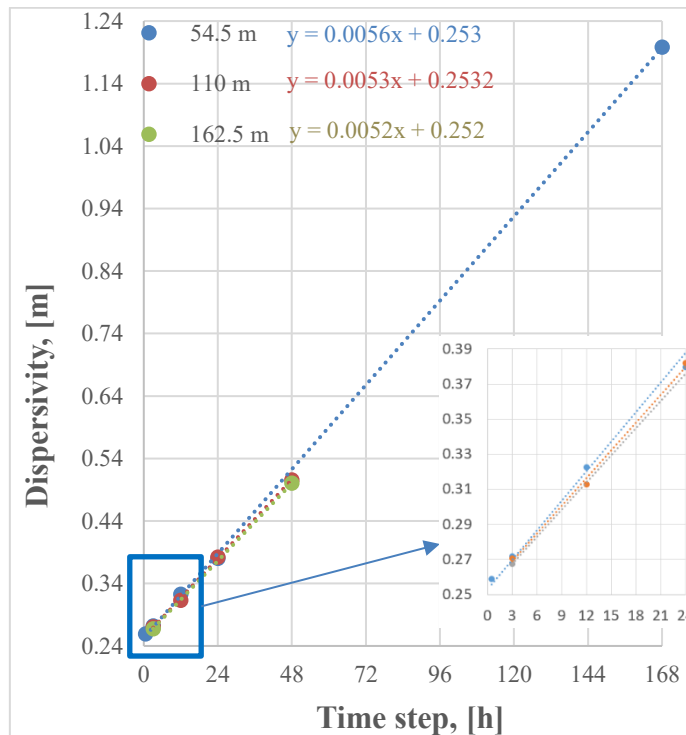


Figure 28. Dispersivity and time-step size correlation for homogeneous models of various sizes

Figure 28 shows the impact of different time-steps on models with different lengths:

- 54.5 m
- 110 m
- 162.5 m

With the following gridding:

- $\Delta x = 0.5$ m
- $\Delta y = 1$ m
- $\Delta z = 0.12$ m

As it was stated earlier, the values for the porosity and permeability in x, y and z directions were taken the mean ones from the heterogeneous model:

- Porosity = 24 %
- Permeability in x-direction = 634 mD
- Permeability in y-direction = Permeability in z-direction = 384 mD

The injection rate for this model and all the further models was 1.44 m³/day. The well rules (well operating limitations) were always set in such a way that the liquid injection rate and liquid production rate were the same. Bottom hole pressure limit was set to 50 bar.

The dispersivity values used in this plot were the averaged ones.

The extrapolation to almost zero time-step size for all the models gave the same dispersivity value (~ 0.25 m). From the plot, it is obvious that the bigger the time-step used for calculations, the bigger difference between the total dispersivities in the model. As 0.5 hour as a time step size was requiring a very long time for one simulation run, it is recommended to use a time-step within the 3-12 hours range.

Another interesting observation is that short distances possess a slightly higher dependency on the time-step than longer ones.

4.1.4 Single-phase flow in heterogeneous model, tracer in water

4.1.4.1 Impact of the time-step size

It is necessary to choose the right time-step value of the calculations in the simulations to make an adequate observation of the grid-size impact on numerical dispersion. Previous experiments made it clear that the contribution of the wrong time-step size into the numerical dispersion is significant in the homogeneous situation. However, there was no clear evidence if the correlation will be the same in the heterogeneous case, so it was compulsory to make clear which time-step range are the most reasonable for heterogeneous-model simulations.

Figure 29 shows the impact of different time-steps on models with different lengths, as it was done for homogeneous case: 52.5 m, 110 m, 162.5 m (α stands for dispersivity).

The choice of the starting point of 6 hours time-step for the correlations was made based on the results of the previous experiment. As it was stated, the range of 3-12 hours was recommended.

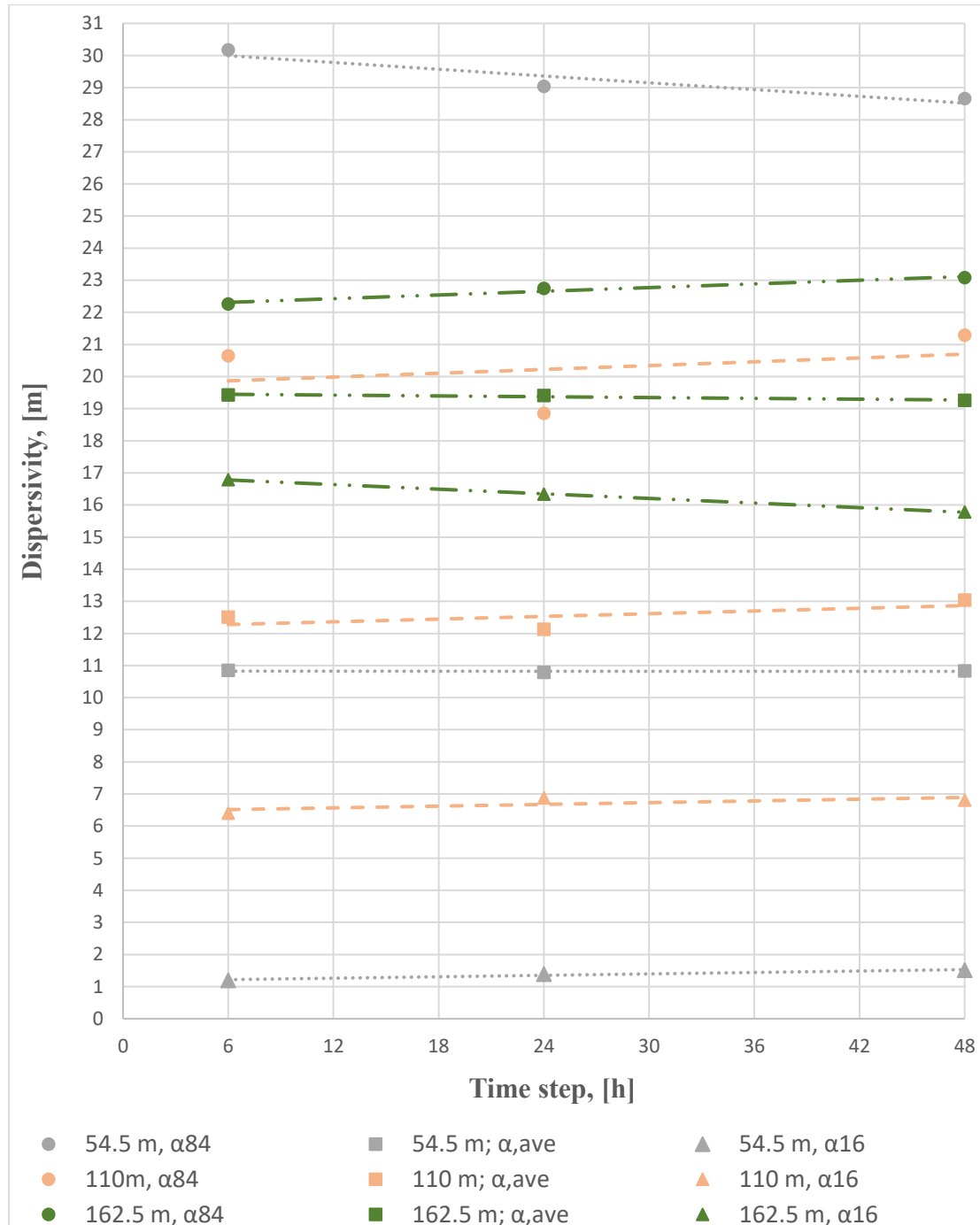


Figure 29. Dispersivity and time-step size correlation for heterogeneous models of various sizes

From the figure, there is no time-step size impact on the dispersivity. The possible explanation of this phenomenon might be the dominating impact of heterogeneity. The starting value of the

dispersivity stays within the range of 1.20 - 30.18 when the homogeneous case had dispersivity values below 0.38 for the recommended time-step range.

Another observation was the increasing symmetry of the C/C_0 curve with the increase of the distance between the wells. The less the range between α_{16} and α_{84} the more symmetrical the curve.

4.1.4.2 Correlation between dispersivity and the flow distance

It is challenging to state the correlation of the dispersivity with distance due to the dissymmetry in the C/C_0 curve, especially in 54.5 well distance, where the dissymmetry is very high (Figure 30). The range ($\alpha_{16} - \alpha_{84}$) for 162.5 m well distance stays within the range for 54.5 m well distance, though the averaged value is increasing.

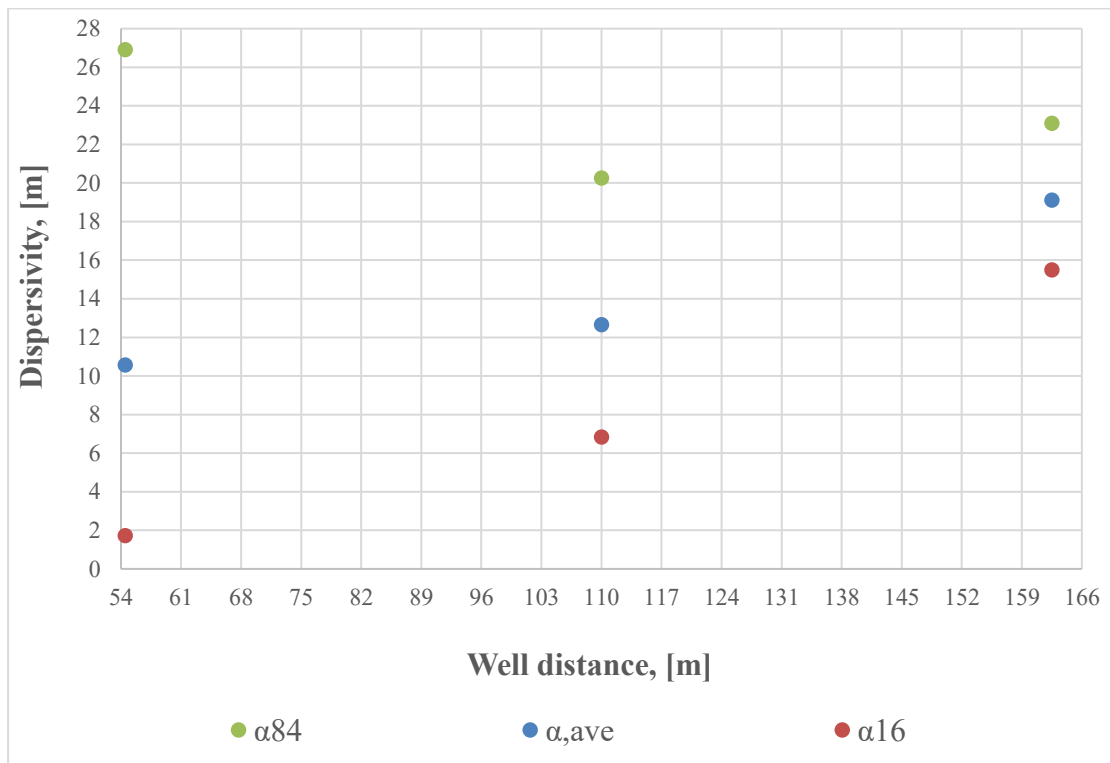


Figure 30. Dispersivity versus well distance, for gridding $\Delta x=1m$, $\Delta z=0,12m$

4.1.4.3 Effect of normal and reverse positions of the injection and production wells on dispersivity

The other way to estimate the impact of heterogeneity is to switch places of the injection and production wells and compare the resulting dispersivities. Figure 31 shows the difference in the dispersivities in correlation with the distance between the wells.

A possible interpretation of the graph is that the first 52.4 m of the model the geological features change very mildly (comparing to the total model), resulting in almost no difference in dispersivities when the injection and production roles of the wells were changed.

Additionally, an increase in the range of $\Delta\alpha$ with the distance was observed.

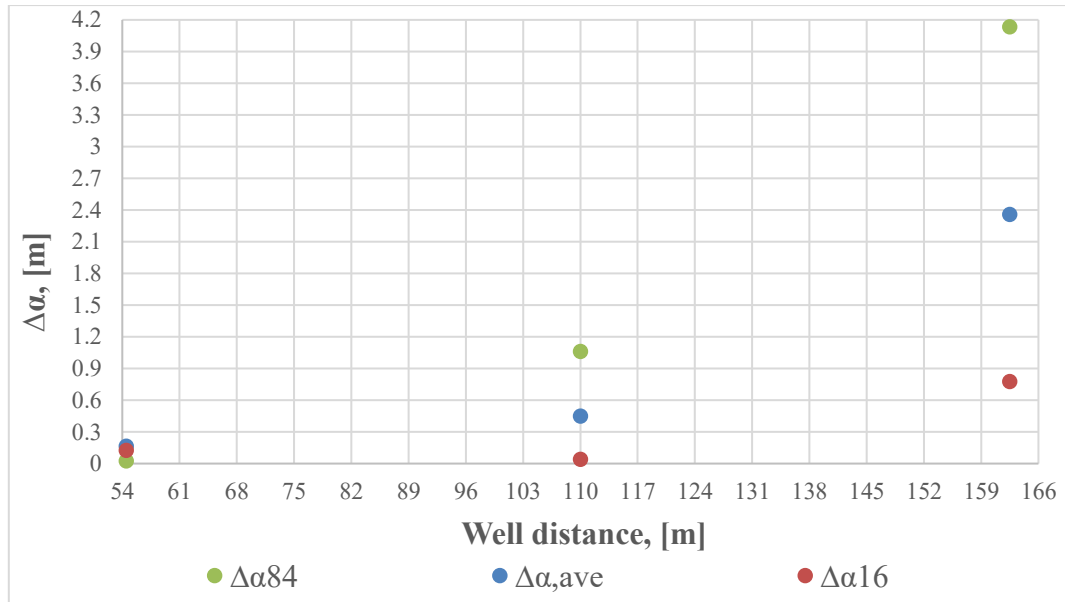


Figure 31. Difference between normal and reverse positions of the injection and production wells

4.1.4.4 Effect of gridding on dispersivity

The investigation of the gridding impact on dispersivity also gave interesting results. As it is seen from Figure 32 - Figure 34 the increase in the grid size in x-direction results in the increase of dispersivity, while the increase in z-direction is decreasing dispersivity.

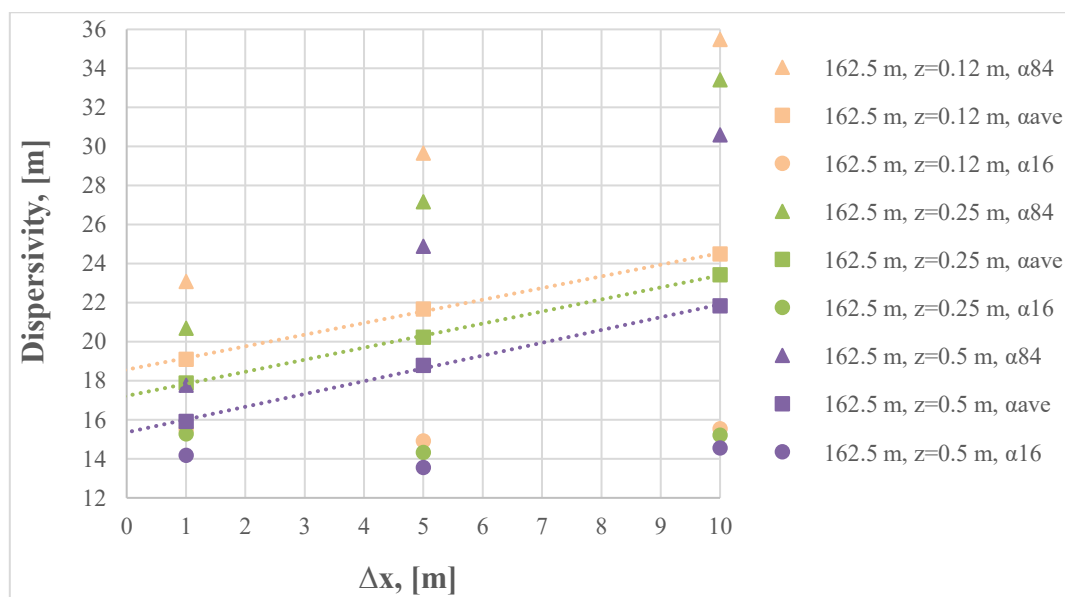


Figure 32. Dispersivity versus grid size for 162.5 m well distance

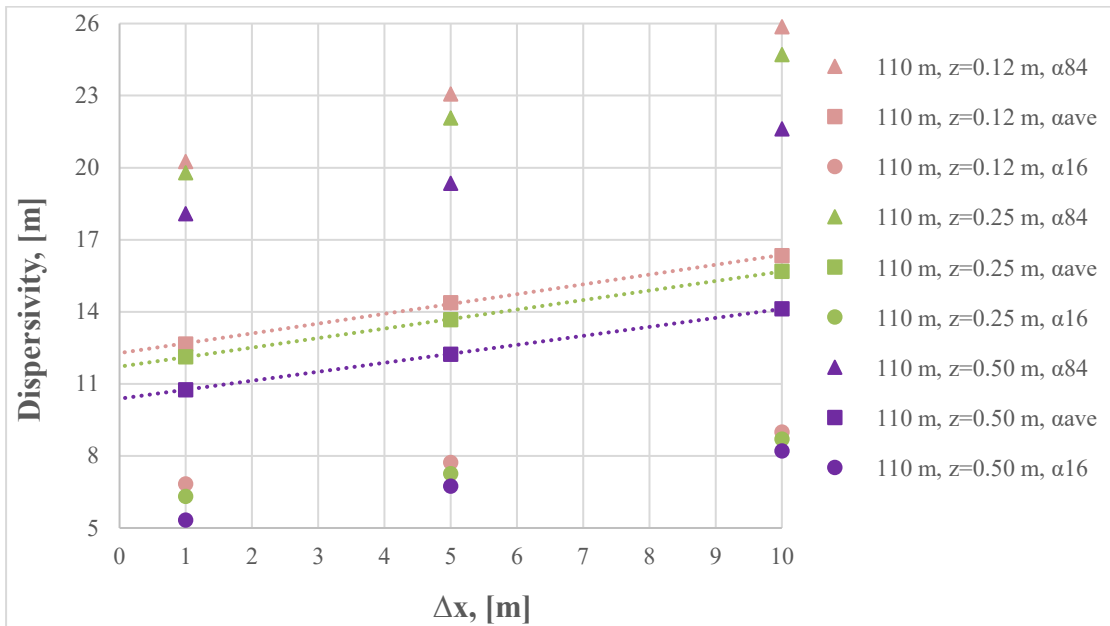


Figure 33. Dispersivity versus grid size for 110 m well distance

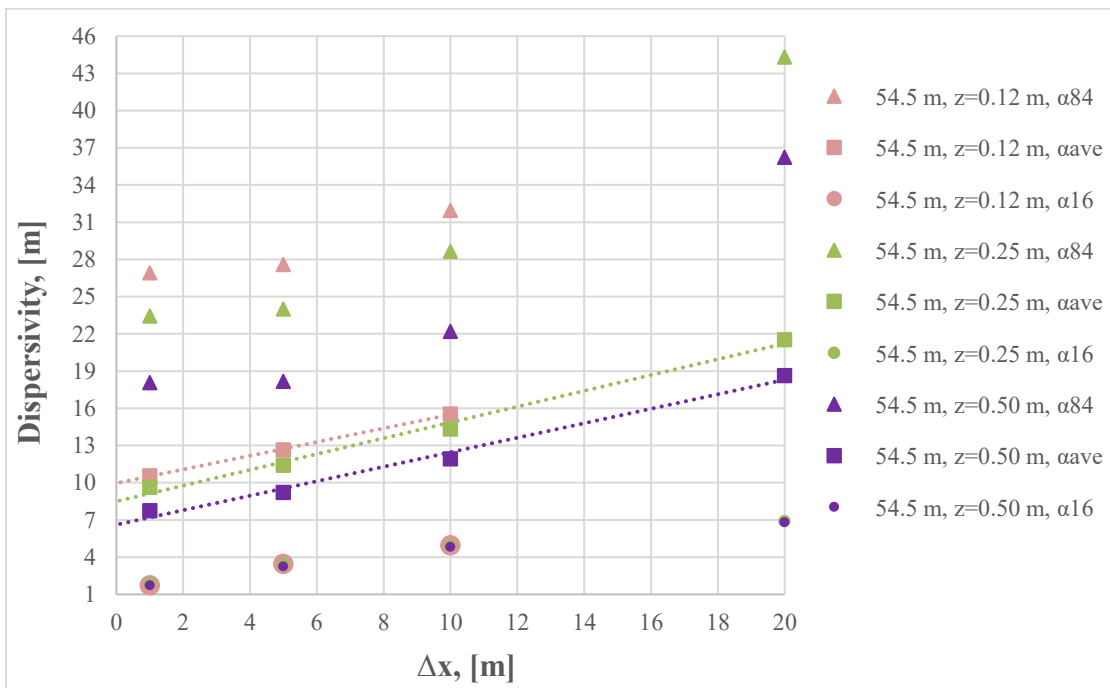


Figure 34. Dispersivity versus grid size for 54.5 m well distance

Other observations are the following:

- the averaged dispersivity has a linear trend with the change of the grid size
- the larger is Δz , the less dispersivity range is observed
- in the 54.5 m case the $\Delta\alpha_{16}$ value stays almost constant with the change of grid in z-direction

4.1.4.5 Dispersion impact on tracer production

As was already stated, for two-dimensional case flow simulation, a tracer slug was injected in the model. This is the explanation that in Figure 35 tracer rate-production increase and decrease can be observed. The section gives an example of a simulated tracer production-rate match for a single-phase flow only.

While the liquid production data for a fine grid-block model ($\Delta x = 0.5$ m and $\Delta z = 0.12$ m) and a bigger one ($\Delta x = 10$ m and $\Delta z = 0.5$ m) had a good match, the tracer production data is not giving such a nice fit (Figure 35).

From the figure, it is obvious that the increase in grid-size has an impact on the smear-out of the curvature. The effect in z-direction is much smaller than in x-direction. In addition, tracer breakout in models with bigger grids happens earlier.

The peaks in the fine-scale model are generated by the rock heterogeneity. It means that the tracer is traveling at different speeds through the different layers. The process of upscaling homogenized the medium and that lead to the reduction of velocity variations in the coarse model comparing to the original one.

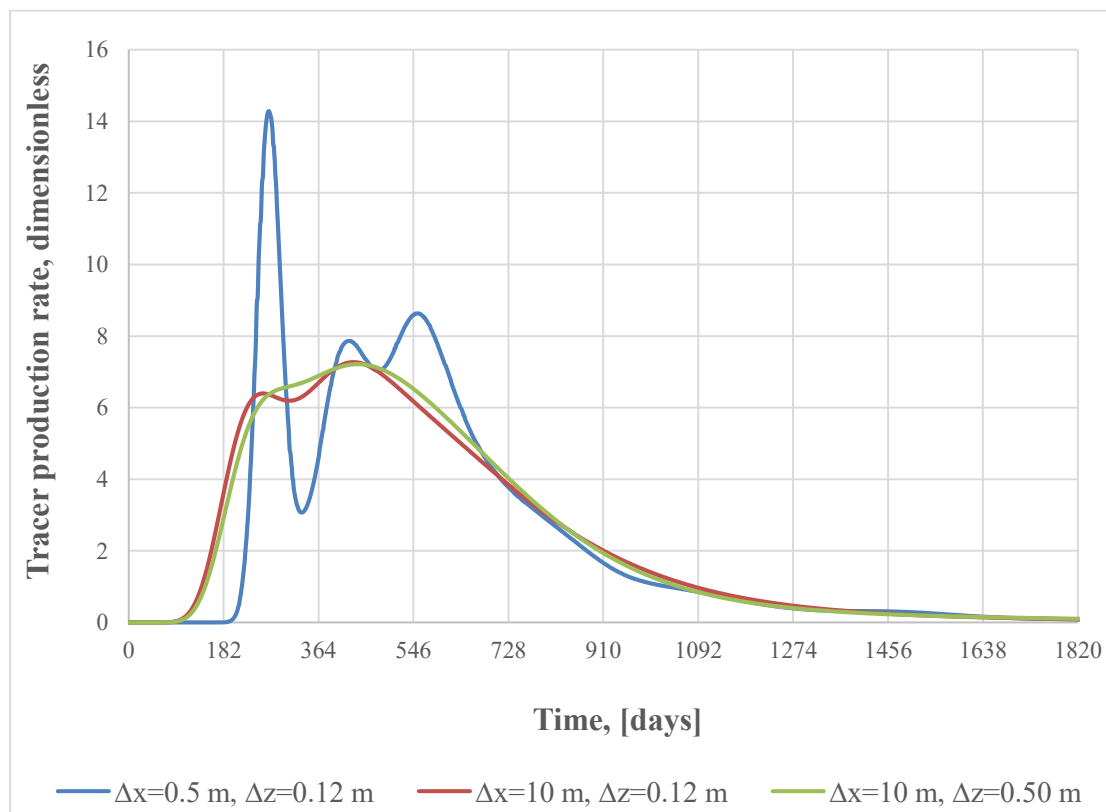


Figure 35. Tracer production concentration for different gridding

Reservoir engineers claim that it is the case for conservative and partitioning tracers. In previous studies performed by OMV (Dominik Steineder), it has been observed that while it is possible

to history match oil production quite well (see Figure 36), the tracer production data is still not well reproduced (Figure 37). Blue and green dots stand for production history data, the rest is the results of simulation models.

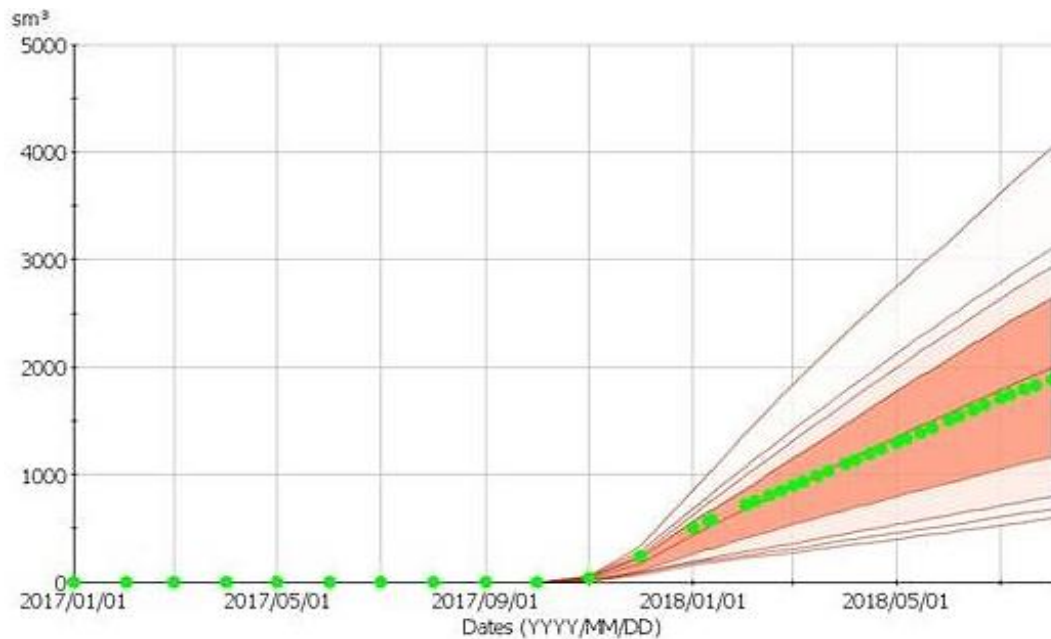


Figure 36. History match. Oil cumulative production
(OMV personal communication, Dominik Steineder, 2019)

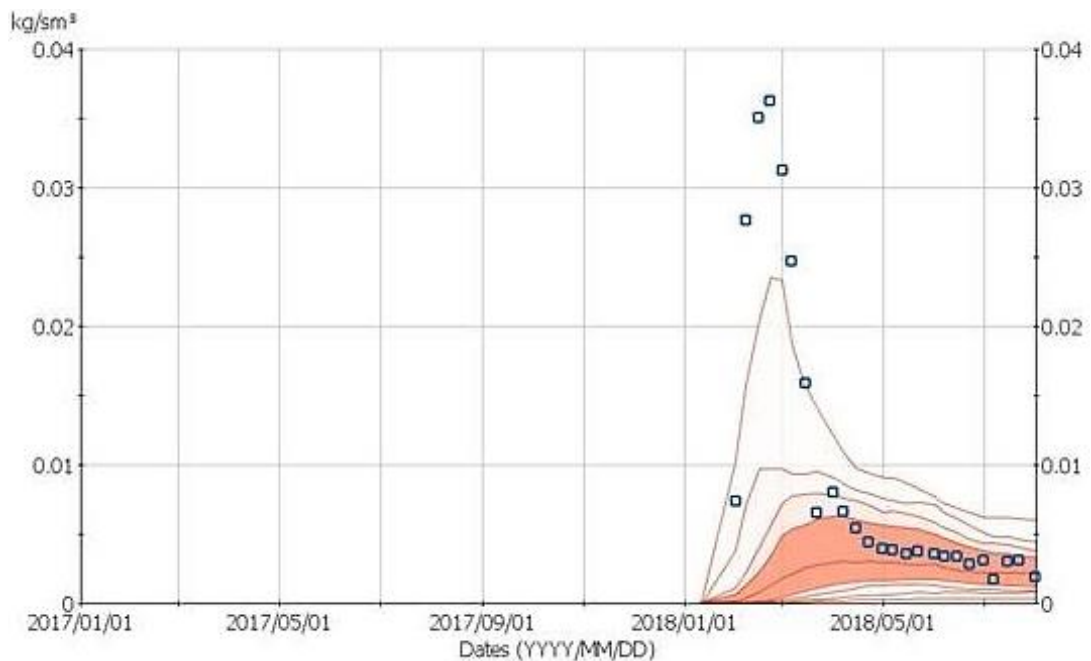


Figure 37. History match. Tracer production rate
(OMV personal communication, Dominik Steineder, 2019)

The examples of tracer production-rate match in a two-phase flow simulation model is given in the next chapter.

4.2 Two-phase flow (oil and water)

Fluid properties for the further models were slightly changed. For example, water was altered to

- 144 bar reference pressure
- 0.42 cP viscosity
- 1.0062 formation volume factor
- 1000.8 kg/m³ density at surface conditions

As it was stated earlier, the work was done only with the dead oil, which has the following properties:

- 50.75 bar reference pressure
- 4.42 cP viscosity
- 868.84 kg/m³ density at surface conditions
- 0.05 kg/m³ density of the solute gas at surface conditions

Simulations were done applying two types of relative-permeability curves, which later will be referred to as “high relative permeability” and “low relative permeability” (Table 3 and Figure 38).

Table 3. High and low relative permeability data input

Sw	High relative permeability, Corey Exponents = 2.5		Low relative permeability, Corey Exponents = 3	
	Krw	Kro	Krw	Kro
1.000	1.000	0.000	1.000	0.000
0.800	0.574	0.000	0.500	0.000
0.733	0.449	0.006	0.351	0.001
0.667	0.340	0.030	0.235	0.005
0.600	0.247	0.073	0.148	0.019
0.533	0.169	0.137	0.086	0.044
0.467	0.106	0.225	0.044	0.086
0.400	0.058	0.336	0.019	0.148
0.333	0.025	0.473	0.005	0.235
0.267	0.006	0.635	0.001	0.351
0.200	0.000	0.825	0.000	0.500

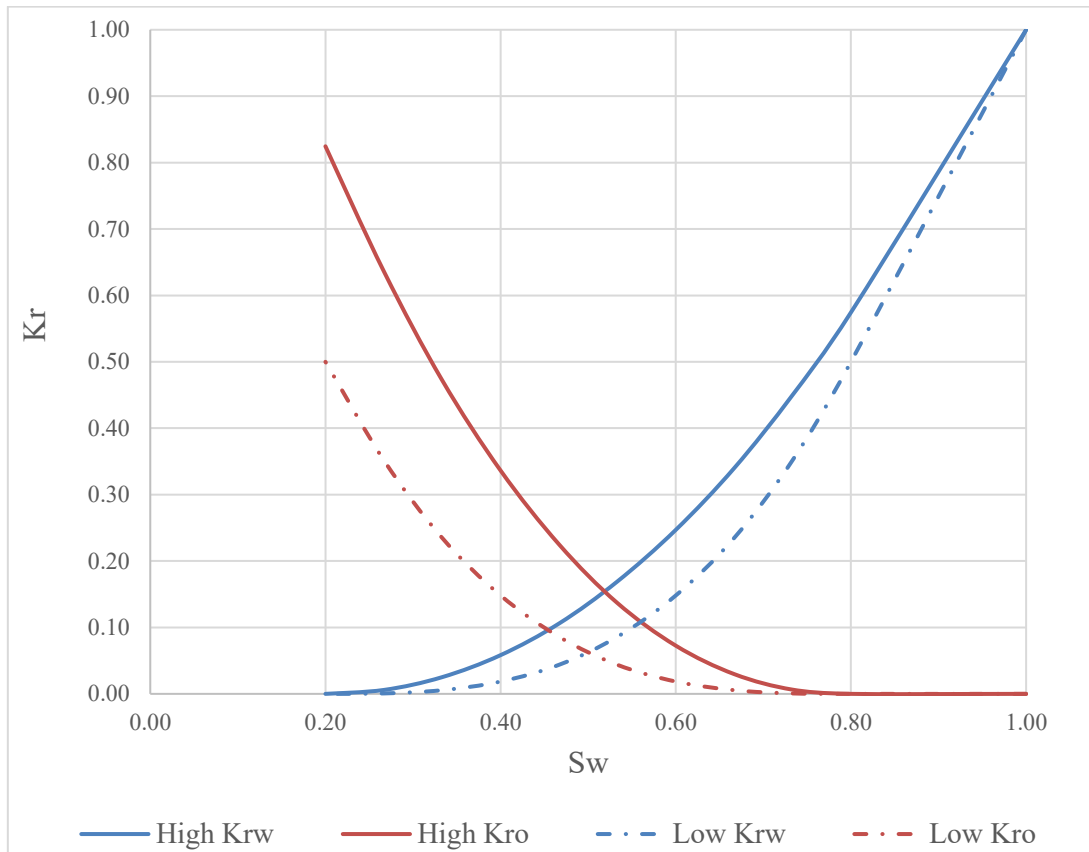


Figure 38. Relative permeability of the two-dimensional flow

4.2.1 Flow in homogeneous permeable 2D media

Simulations on two-phase flow on 54.5 m well distance and 110 m well distance were performed and unlike the one-phase flow, the distance this time had a high impact on dispersion. The bigger the distance the more dispersion happens at the same field average saturation state. Nevertheless, the biggest change in dispersivity is induced by relative permeability functions. In the high relative permeability case, the dispersivity has much higher values. However, the closer the system to residual oil saturation, the more alike the dispersion in the system.

Figure 39 describes the velocity decrease with the increase of field average saturation; Figure 40 gives a description of the dispersivity change. The simulation run was performed by injecting tracers in water, one tracer after the other. Gridding for the cases displayed on the two figures below was the same: $\Delta x = 0.5$ m, $\Delta z = 0.12$ m.

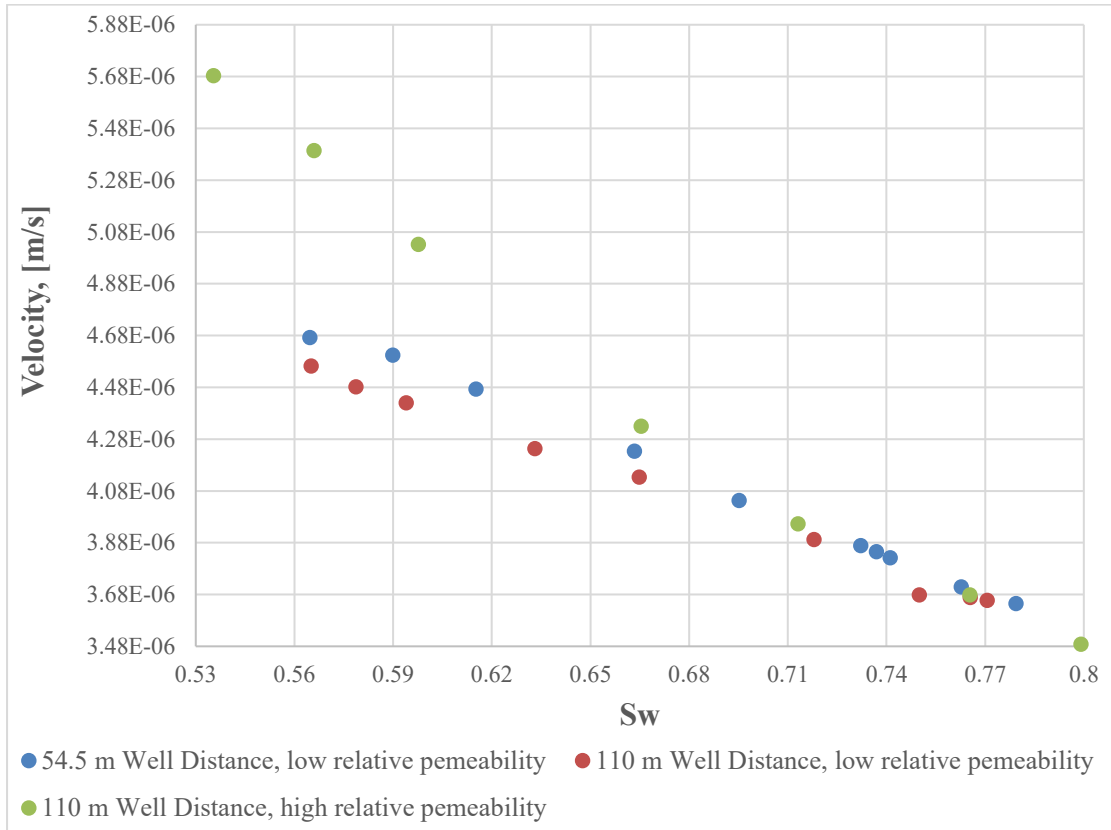


Figure 39. Velocity versus field average saturation

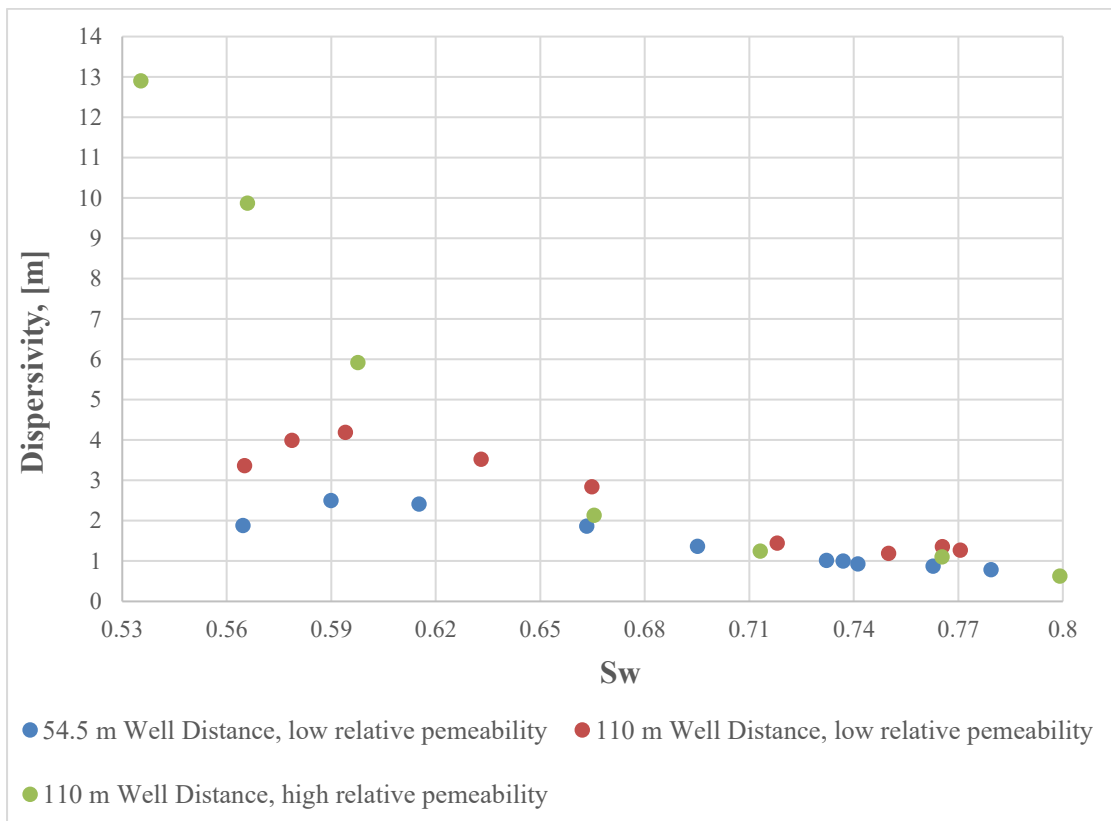


Figure 40. Dispersivity versus field average saturation

4.2.2 Flow in heterogeneous permeable 2D media

The impact of gridding is very interesting for the two-phase flow in the heterogeneous media. While there is not much of a difference between $\Delta x = 1$ m, $\Delta z = 0.12$ m and $\Delta x = 5$ m, $\Delta z = 0.5$ m, when the simulation is performed in the typical gridding range (10-20 m in x-direction), the total dispersivity is much higher (Figure 42). However, the velocities depending on gridding do not differ much (Figure 41).

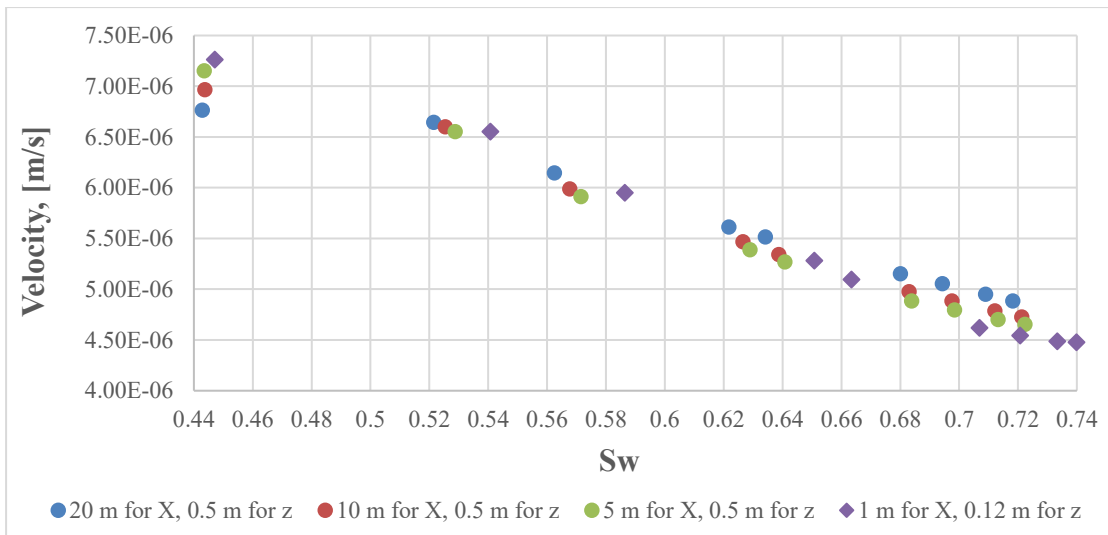


Figure 41. Velocity versus heterogeneous field average saturation

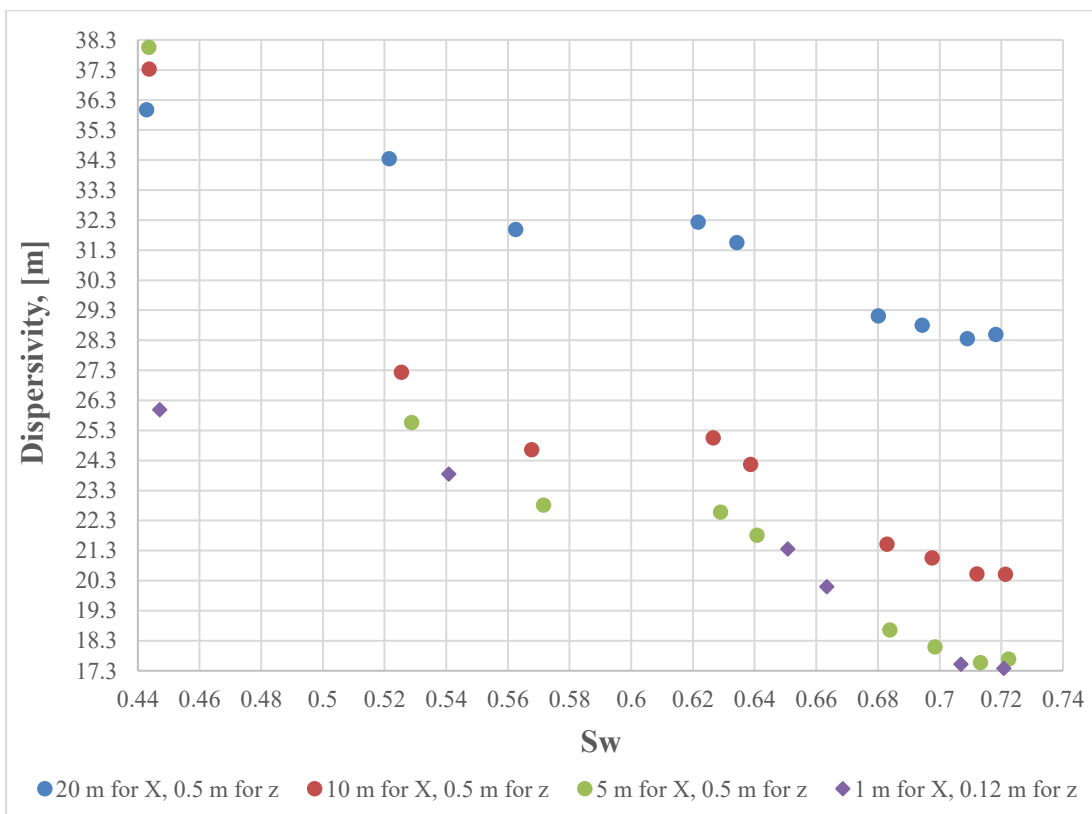


Figure 42. Dispersivity versus heterogeneous field average saturation

4.3 Two-phase flow with alkaline-polymer

Until now, the investigation was answering mainly to three questions:

- What are dispersion and dispersivity?
- What properties of the simulation model change them?
- How do those properties change dispersion and dispersivity?

The question of how dispersion influence the forecast of incremental oil recovery was not discussed yet.

During the two-phase flow simulation, gridding change did not seem to have a significant impact on the production rates or pressures. However, for the forecast of oil-recovery after the alkaline-polymer flood, the situation is different. The difference in the forecasts is shown in table Table 4 and Figure 43.

Table 4. Oil recovery after alkaline-polymer flooding

Cell size	$\Delta x = 20 \text{ m}; \Delta z = 0.5 \text{ m}$	$\Delta x = 1 \text{ m}; \Delta z = 0.12 \text{ m}$
Pore volume	948	947
Oil Originally in Place, m³	748	747
Oil After Water Flood, m³	299	282
Oil After Chemicals, m³	210	167
RF After Water Flood	0.60	0.62
RF After Chemicals	0.72	0.78

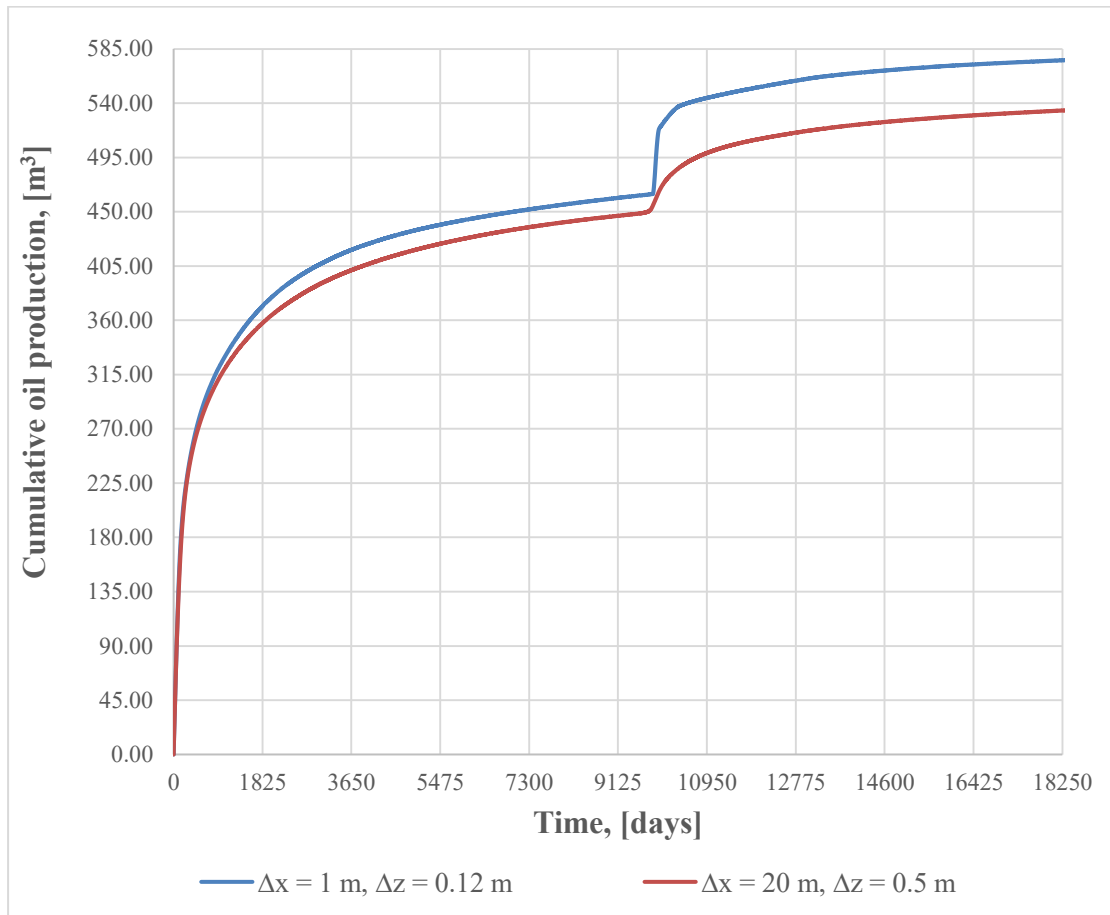


Figure 43. Oil recovery

As can be seen in the Table 4, the predicted oil recovery after both the water flood as well as after the chemical injection for larger grid model differ from the predicted oil recovery for a finer-grid model: with the smaller gridding, the recovery factor increases from 62% after the water flood, to 78% after the chemical injection, for an incremental production of 16 percentage points, or a relative increase of 26%. With the larger gridding, the recovery factor increases from 60% to 72%, for an incremental production of 12 percentage points, or a relative increase of 20%.

Chapter 5 History matching

The previous two chapters proved, that introduction of the finer grid gives the opportunity of more precise forecasts but even though the computational power nowadays is rapidly developing and engineers are able to create their models with finer and finer grids, this resource is still limited. Therefore, it is necessary to come up with other approaches of getting to precise history match and production forecasts.

5.1 Relative-permeability pseudo-functions

Mattax and Dalton (1990) described in their book the method of relative-permeability pseudo-functions. However, the described in this master-thesis reservoir-model, gridding increase is not having a significant impact on the water-rate behavior (Figure 44).

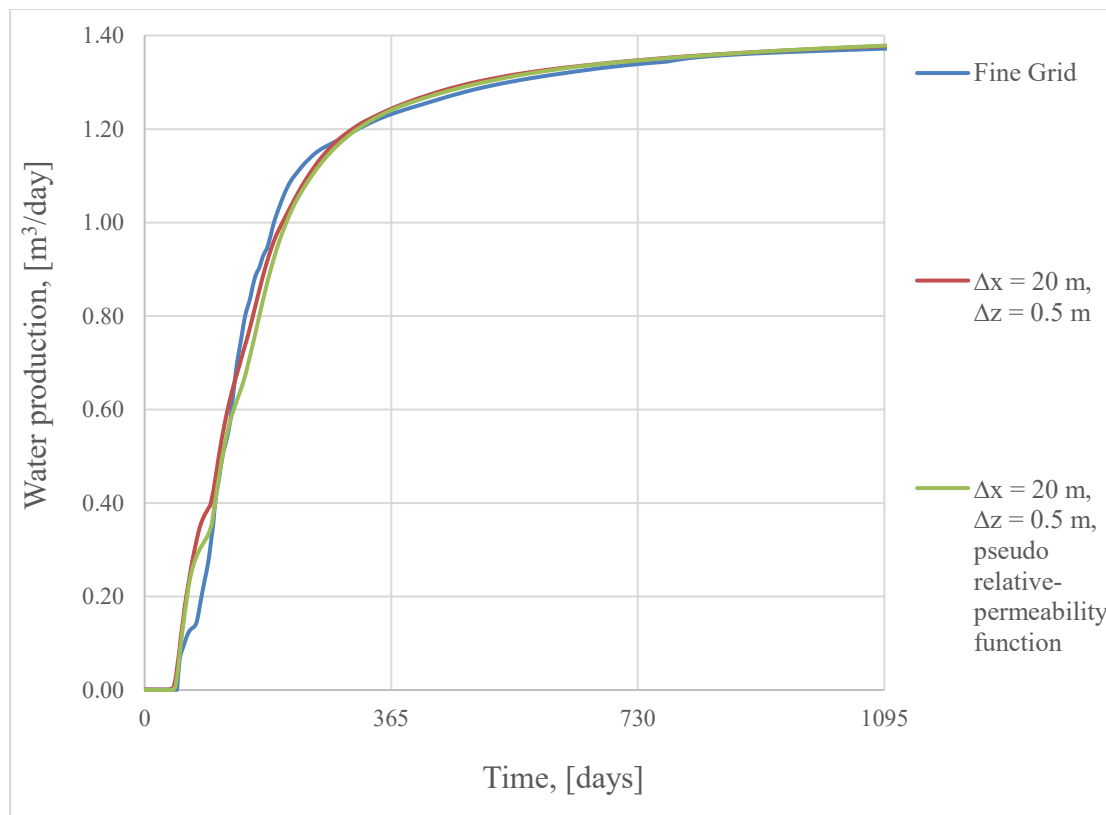


Figure 44. Water production rate of models with different gridding and relative-permeability functions

The only one pseudo-functions that improved the water-rate match not only did not reproduce the tracer production-rate curve but even hardly changed it (Figure 44 and Figure 45).

As tracer injection lasted only one month in the simulation, tracer production-rate increase and decrease is observed in Figure 45. The peaks in the fine-grid model are generated by the rock heterogeneity, the tracer is traveling at different speeds through the different layers. Grid-upscaling homogenized the properties of the model and the tracer velocity variation decreased. Truncation error also induced rapid saturation change, therefore earlier tracer-breakthrough is observed in the coarse-grid model.

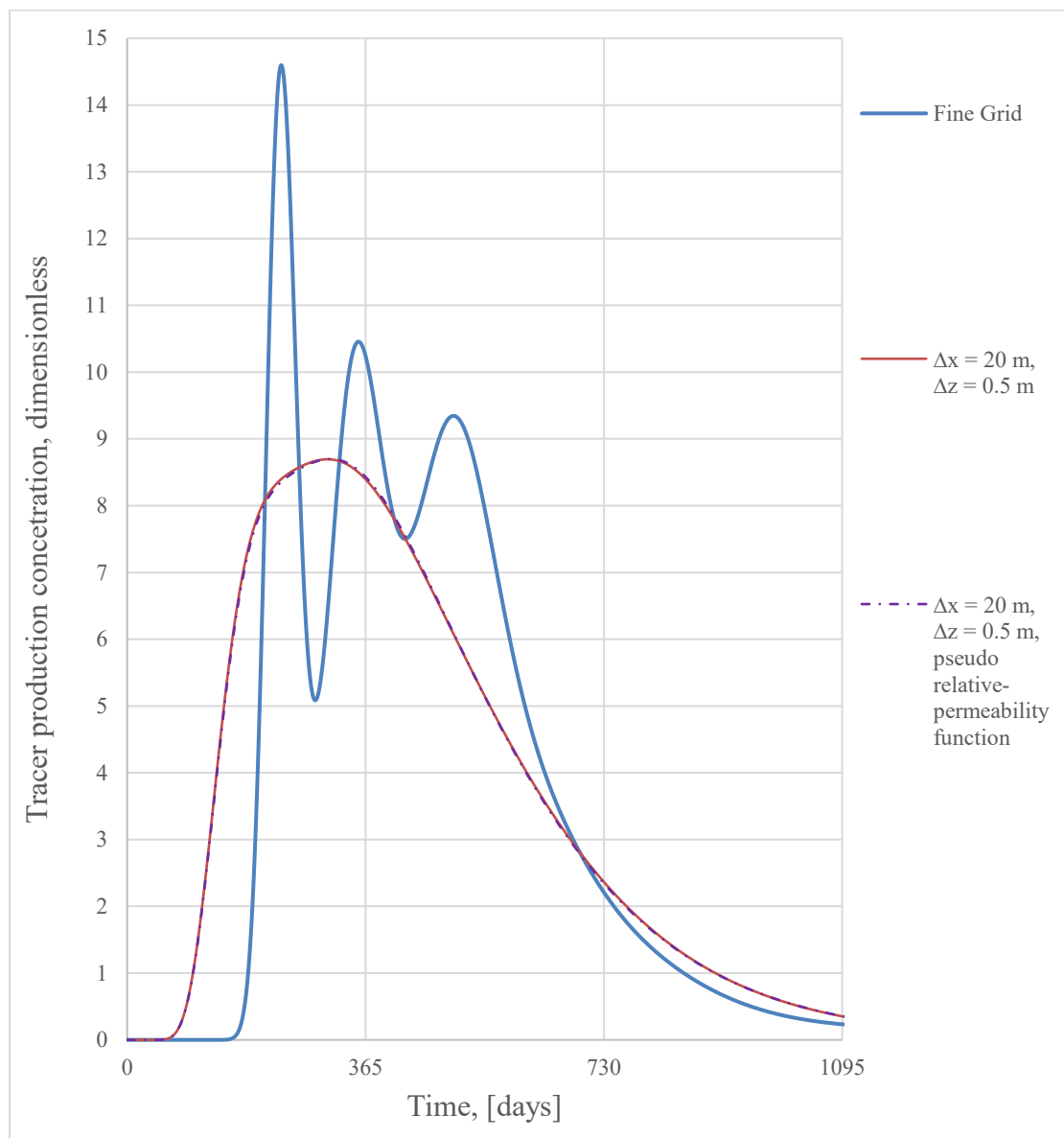


Figure 45. Tracer production rate of models with different gridding and relative-permeability functions

A remark for the two last figures should be mentioned: the timeline in Figure 44 starts since the beginning of water injection, while the timeline in Figure 45 starts since the injection of tracer 6.

Tracer 6 is injected after almost 26 years of water injection when the water production rate for all three models is the same.

5.2 Diffusion control

Another way to match water production-rate that is provided by Eclipse is diffusion control.

This option reproduced water production-rate quite precisely (Figure 46) and significantly improved the tracer production-rate match (Figure 47). The tracer breakthrough time of the coarser-grid model was shifted much closer to the breakthrough time of the finer-grid model. The diffusion control option enabled to reproduce the rate-production peaks. Nevertheless, there is still room for improvement for tracer curve reproduction.

A reservoir model that is able to reproduce tracer production-rate should also improve incremental oil forecast for an alkaline-polymer flood but Eclipse uses this “diffusion control” option to solve tracer-equation only. It will not help in production forecasts.

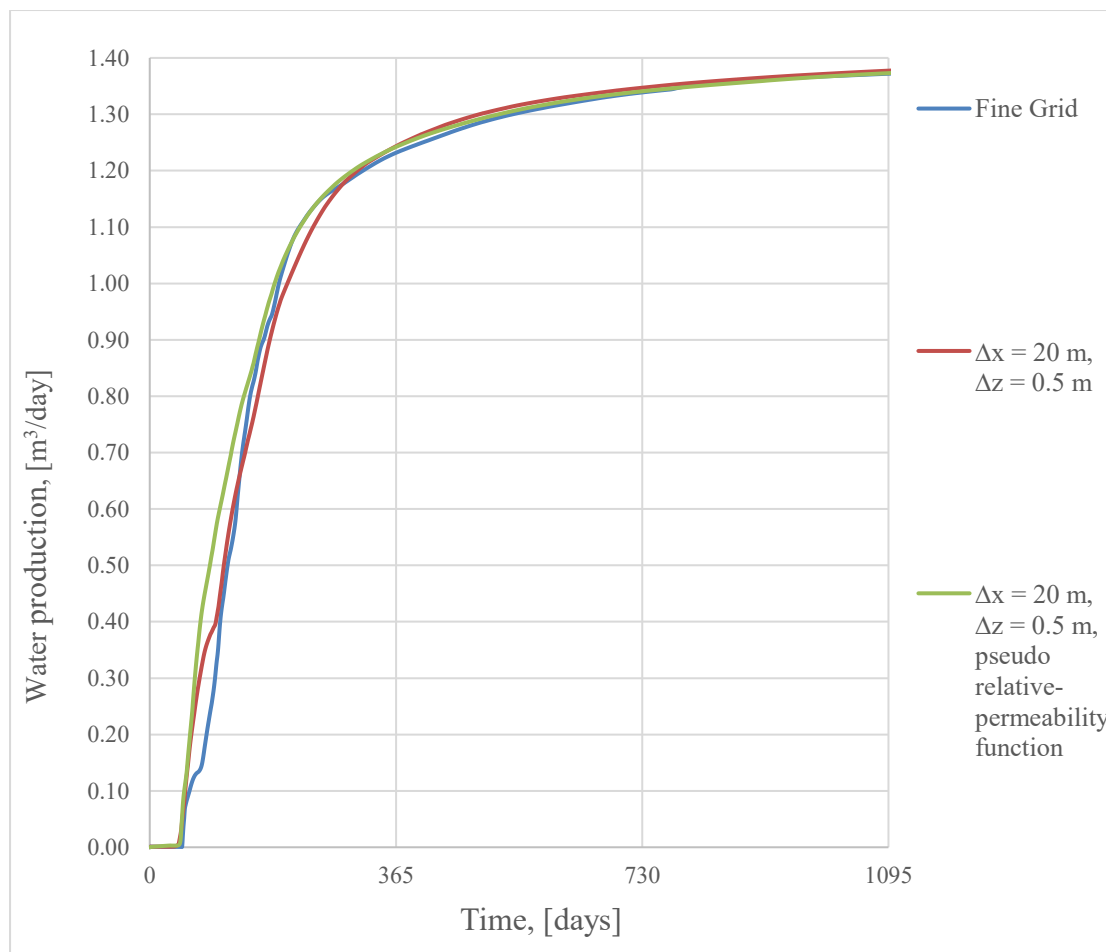


Figure 46. Water production rate of models with different gridding and relative-permeability functions and diffusion control option switched on

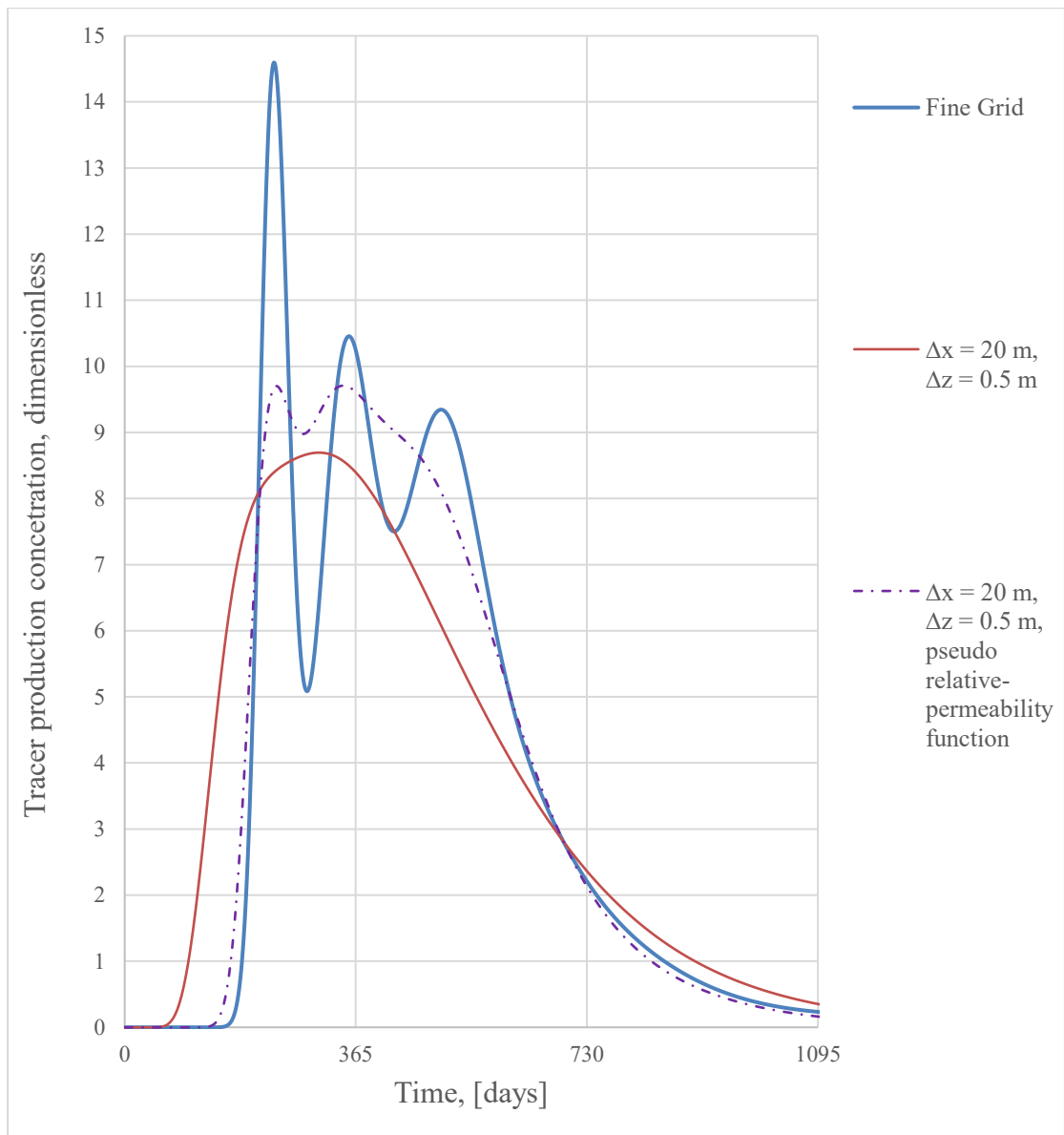


Figure 47. Tracer production rate of models with different gridding and relative-permeability functions and diffusion control option switched on

Chapter 6 **Results and Discussion**

Even though all of the results have already been mentioned above, it is necessary to give a short overview of what was achieved to make the result discussion more clear.

6.1 1D homogeneous single-phase flow models

The investigation has proven the correlation of Herzer and Kinzelbach (1989): dispersivity is equal to the half of the grid-block size in x-direction in a fully homogeneous model with a single-phase flow. However, the wrong calculation time-step (a too big one) influences the result, making the dispersivity bigger than half of the grid-block. Thereby, it is important to watch out for the input data of the calculation time-step.

The equation 3.1.12 is true only for a fully homogeneous case, which does not exist in reality. Even the cores that are considered to be homogeneous are not perfectly fulfilling this condition. Therefore, to achieve the simulated tracer-production data match with laboratory tracer-test, the grid-block size and time-steps should be adjusted in the perfectly homogeneous simulation model. This technique will allow mimicking the physical dispersion with numerical dispersion.

Porosity change influences on the interstitial velocity of the flow and therefore has an impact on dispersion.

6.2 1D homogeneous two-phase flow models

Two main observations were achieved by running simulations of a water-flood in homogeneous fully oil-saturated core-models:

1. Dispersion and dispersivity values in the low oil-viscosity case were higher than in the high oil-viscosity case
2. The closer the model is to the residual oil saturation state, the closer the dispersivity is to the relation described by the equation 3.1.12. This observation is applicable to both oil-viscosities.

The last observation is also true in the case of an alkaline-polymer flood. When the system reaches the state of none movable oil left, the mentioned above dispersivity correlation with the grid-block size exists as the system again has only single-phase flow.

6.3 2D homogeneous single-phase flow models

The calculation time-step size is having a significant impact on dispersion and dispersivity in this type of models. Dispersivity values proved to be ~half of the grid-block size in x-direction in the situation when a small calculation time-step is used (less than 30 minutes). However, the simulations with such small time-steps take more than two hours of runtime. The dispersivity increase with the increase of the time-step trend is linear.

One more observation is that short flow-distances between the wells has a slightly higher dependency on the time-step than longer ones.

As the simulated model is small, it seems unreasonable to use calculations time-step size less than of 3 hours, as it is very unpractical to have such a long simulation-run for such a small part of the reservoir. Of course, this is relevant in case of the application of gridding as small as described in the thesis in section 0.

6.4 2D heterogeneous single-phase flow models

These types of models give a nice spectrum of observations:

1. Dispersivity values increased significantly with the introduction of heterogeneity. However, the impact of the time-step size is not clear.
The values stayed within the range of 1.20 - 30.18, while in the homogeneous case dispersivity values are below 0.38 if the simulations have the calculation time-step within the recommended range.
The averaged dispersivity increases with the increase in the flow distance between the wells.
2. When α_{16} is equal to α_{84} the curve C/C_0 is symmetrical. The simulations showed that the bigger the distance between injection and production wells, the closer the α_{16} and α_{84} values, therefore the more the observed symmetry in the C/C_0 curve.
3. Due to the present dissymmetry in the C/C_0 curve, it is hard to judge the correlation between dispersivity and the flow distance. The averaged dispersivity increases with the increase of the flow distance.

4. The injection and production roles of the wells were changed and compared to the dispersivities in the initial flow directions. $\Delta\alpha$ increased with the increase of the distance between the wells.
5. An increase in the grid-block size in x-direction (Δx increase) led to an increase in dispersivity values. The increase in the averaged dispersivity values has a linear trend.
6. An increase in the grid-block size in z-direction (Δz increase) led to a decrease in dispersivity values. The decrease in the averaged dispersivity values has a linear trend.

The impact of the calculation time-step size is not clear probably due to the significant heterogeneity impact on dispersion.

$\Delta\alpha$ increased with the increase of the distance between the wells could be explained by the increase of the reservoir heterogeneity with the flow distance.

Change of the grid-block size has an important impact on the numerical dispersion in these types of models, thereby the size should be chosen carefully.

6.5 2D two-phase flow models

The overall observation of the homogeneous type of these models is: the less the amount of the movable oil in the system, the less is the range between dispersivity values of the systems. However, this is not the case for the heterogeneous situation.

The dispersivity trend for models with $\Delta x=1$ m and $\Delta x=5$ m looks very alike but this can be the result of a larger Δz value in the second model. In cases with equal Δz value, the observation shows the increase of dispersivity with the increase of Δx .

The impact of gridding in the heterogeneous case is even greater than in the homogeneous. Therefore, the grid-size in the first case should be chosen with even more care, than in the second one, even though it has no influence on the water-cut results.

Models with an increased size of grid-blocks were very good in terms of water-cut reproduction but in terms of tracer-concentration production-rate rate curve reproduction, they failed. The curves were highly smoothed. Reservoir engineers at OMV also experience this problem while trying to history-match tracer-tests.

The comparison of alkaline-polymer simulation runs of models with different grid-block sizes revealed a different result of incremental oil recovery from the model with bigger grid-blocks.

Fine gridding showed a 6% higher recovery factor after the alkaline-polymer flood than the typical grid-size for full-field simulations. The underestimation of incremental oil-recovery may lead to the underestimation of the profitability of any EOR project and that is obviously

leading to the wrong decisions of running the project or not. In other words, a profitable project might be declined due to the wrong grid-block size chosen for a forecast simulation.

The gridding size affects Darcy velocity and Darcy velocity affects capillary number:

$$N_c = \frac{\mu v}{\sigma_{ow}} \quad (6.5.27)$$

Where

σ_{ow} = interfacial tension

μ = viscosity

v = Darcy velocity

Capillary number in return effects oil saturation state of the system.

To improve oil-recovery forecasts tracer-curve match should be improved. However, in the Eclipse manual, it is stated that the diffusion control option is applied for tracer equations solutions. The other dispersion and diffusion control options provided by Eclipse are also only improving the solution of the tracer equation. Right now Eclipse does not have any improving solution for surfactant and polymer floods.

6.6 History match

The long-ago published techniques of introducing relative-permeability pseudo-functions were mainly making the water-cut match worse (20 different pseudo-functions were used). The only one that maintained the quality of the match did not make any changes in terms of tracer production-curve match.

The diffusion control option for the TRACERS keyword in RUNSPEC section in Eclipse simulation file provided an improved tracer production-curve match with maintained quality of the total water production-curve match. However, the diffusion-control option is used only in solving the tracer equation by Eclipse. This option does not change the recovery forecasts.

Chapter 7 Conclusion

It was proven that numerical dispersion has a significant effect on the results of simulation runs and it also can be used to mimic the physical (real) dispersion.

7.1 Summary

It was observed that for homogeneous models time-step size has a significant impact on the sharpness of breakthrough fronts, while in heterogeneous models it is not so important. Fluid properties also should be chosen carefully, as they affect the total simulated dispersion

However, grid-block size affects all types of models. The effect is very important for the industry because it has an impact on the incremental oil-recovery forecasts for alkaline-polymer projects. The work performed in the frame of this master thesis showed that different grid-block size lead to different forecast of oil recovery after alkaline-polymer flood. However, there was almost no effect on water-cut. Therefore, the relative-permeability pseudo-function application did not improve the situation.

Even though Eclipse provides options for diffusion and dispersion control, all of them are used only in tracer-equation solutions. Those options will not improve the forecasts.

7.2 Evaluation

Dispersion and dispersivity effects were observed in a wide range of possible situation. Starting from single-phase core flood simulations and finishing with 2D field-cross section simulation of an alkaline-polymer flood.

7.3 Future Work

It is important to make an evaluation of how reliable the averaged dispersivity values are. This evaluation will help to make conclusions concerning the correlation of the dispersion with the flow distance between the wells.

The reliability of the simulation data should be proven with a field test.

List of Figures

Figure 1. Saturation averaging in a cell	12
Figure 2. Tracer displacement of a resident fluid in a capillary tube.....	17
Figure 3. Error function	19
Figure 4. Complementary error function	19
Figure 5. Longitudinal dispersivity versus scale with data classified by reliability	20
Figure 6. Core-plug dimensions.....	22
Figure 7. Dispersion versus reverse number of grid blocks.....	24
Figure 8. Dispersivity versus reverse number of grid blocks	25
Figure 9. Velocity correlation with porosity	26
Figure 10. Velocity correlation with the reverse value for porosity	26
Figure 11. Relative-permeability functions for the two-phase flow in homogeneous media ..	27
Figure 12. Dispersion versus sample average water saturation.	28
Figure 13. Dispersivity versus sample average water saturation.	28
Figure 14. Velocity versus sample average water-saturation.....	29
Figure 15. Calculation of the relative permeability, Eclipse manual.....	31
Figure 16. Injection schedule.....	32
Figure 17. Dispersivity versus sample average water saturation during AP flood	33
Figure 18. Dispersion versus sample average water saturation during AP flood	34
Figure 19. Permeability versus porosity functions.....	36
Figure 20. Interpolated Rock-type distribution between BO_157 and BO_81.....	37
Figure 21. Data analysis for facies.....	38
Figure 22. Fine-model porosity distribution	39
Figure 23. Fine-model permeability distribution	39
Figure 24. Permeability distribution for gridding size	40
Figure 25. Permeability distribution for gridding size	41
Figure 26. No-flow boundary condition for coarse cell.....	41
Figure 27. Tracer relative production curve.....	43
Figure 28. Dispersivity and time-step size correlation for homogeneous models	44
Figure 29. Dispersivity and time-step size correlation for heterogeneous models	46
Figure 30. Dispersivity versus well distance, for gridding $\Delta x=1\text{m}$, $\Delta z=0,12\text{m}$	47
Figure 31. Difference between normal and reverse injection and production roles	48
Figure 32. Dispersivity versus grid size for 162.5 m well distance	48
Figure 33. Dispersivity versus grid size for 110 m well distance	49
Figure 34. Dispersivity versus grid size for 54.5 m well distance	49
Figure 35. Tracer production concentration for different gridding.....	50
Figure 36. History match. Oil cumulative production	51
Figure 37. History match. Tracer production rate.....	51
Figure 38. Relative permeability of the two-dimensional flow	53
Figure 39. Velocity versus field average saturation.....	54
Figure 40. Dispersivity versus field average saturation.....	54

Figure 41. Velocity versus heterogeneous field average saturation.....	55
Figure 42. Dispersivity versus heterogeneous field average saturation.....	55
Figure 43. Oil recovery.....	57
Figure 44. Water production rate of models with different gridding and relative-permeability functions.....	58
Figure 45. Tracer production rate of models with different gridding and relative-permeability functions.....	59
Figure 46. Water production rate of models with different gridding and relative-permeability functions and diffusion control option switched on.....	60
Figure 47. Tracer production rate of models with different gridding and relative-permeability functions and diffusion control option switched on.....	61

List of Tables

Table 1. Summary of 1D homogeneous single-phase flow simulation-runs results	23
Table 2. Relative permeability input.....	27
Table 3. High and low relative permeability data input.....	52
Table 4. Oil recovery after alkaline-polymer flooding	56

References

- Arya, A., Hewett, T.A., Larson, R.G. et al. (1988). Dispersion and Reservoir Heterogeneity. *SPE Res Eng 3 (1): 139–148. SPE-14364-PA. <http://dx.doi.org/10.2118/14364-PA>.*
- Bear, J. (1972). *Dynamics of Fluids in Porous Media*. New York: Elsevier.
- Blackwell, R.J. (1959). Experiments on mixing by fluid flow in porous media. *Proceedings of Amer. Inst. Chem. Eng. and Soc. Petrol. Eng. 29*.
- Chandrasekara, B. C., Rudraiah, N., and Nagaraj, S. T. (1980). Velocity and Dispersion in Porous-Media. *Eng. Sci., 18*, 921-929.
- Coats, K. H., Whitson, C. H. and Thomas, L. K. (kein Datum). *Modeling Conformance as Dispersion*. SPE Annual Technical Conference and Exhibition, Houston, 26-29 September 2004.
- de Josselin de Jong, G. (1958). Longitudinal and transverse diffusion in granular deposits. *Transactions of the American Geophysical Union 39*, 67-74.
- Escuder, R., Fraile, J., Jordana, S., Ribera, F., Sánchez-Vila, X., Vázquez-Suñé, E. (2009). *Hidrogeología. Conceptos básicos de hidrología subterránea*. Barcelona: Fundación centro internacional de hidrología subterránea.
- Fouda, M. A. (2016). *Relative Permeability Upscaling for Heterogeneous Reservoir Models*. Edinburgh : Heriot-Watt University.
- Garmeh, G., Johns, R.T., and Lake, L.W. (2009). Pore-Scale Simulation of Dispersion in Porous Media. *SPE J. 14 (4): 559–567. SPE-110228-PA. <http://dx.doi.org/10.2118/110228-PA>.*
- Gelhar, L.W., Claire, W., Kenneth, R.R. (1992). A Critical Review of Data on Field-Scale Disperion in Aquifers. *Water Resources Research, vol.28, No 7, S. 1955-1974*.
- Haajizadeh, M., Fayers, F.J., and Cockin, A.P. (2000). *Effects of Phase Behavior, Dispersion and Girding on Sweep Patterns for Nearly Miscible Gas Displacement*. Presented at the SPE Annual Technical Conference, Dallas, 1–4 October: SPE-62995-MS. <http://dx.doi.org/10.2118/>.

- Harleman, D. R. F., Melhorn, P. F., and Rumer, R. R. (1963). Dispersion-Permeability Correlation in Porous Media. *J. Hydraul. Div. Am. Soc. Civ. Eng.*, 67–85.
- Herzer, J., Kinzelbach, W. (1989). Coupling of transport and chemical processes in numerical models. *Geoderma*, 115-127.
- Jha, R.K., Bryant, S.L., Lake, L.W. (2006). Investigation of pore-scale (local) mixing. *Presented at the SPE Improved Oil Recovery Symposium, Tulsa, 22–26 April. SPE-99782-MS. <http://dx.doi.org/10.2118/99782-MS>.*
- John, A.K., Lake, L.W., Bryant, S. et al. (2010). Investigation of Mixing in Field-Scale Miscible Displacements Using Particle-Tracking Simulations of Tracer Floods With Flow Reversal. *SPE J. 15 (3): 598–609. SPE-113429-PA. <http://dx.doi.org/10.2118/113429-PA>.*
- Khalid Aziz. (1993). Reservoir Simulation Grids: Opportunities and Problems. *JPT*, 658-663.
- Lake, W. L. (1989). *Enhanced Oil Recovery*. Englewood Cliffs, New Jersey: Prentice Hall.
- Lake, W. L., Kocurek, A. G., Miller, A. M. (1987). *A systematic procedure for reservoir characterization*. Austin.
- Lantz, R.B. (1971). *Quantitative Evaluation of Numerical Diffusion (Truncation error)*. *SPE J. 11 (3): 315–320. SPE-2811-PA. <http://dx.doi.org/>.*
- Mahadevan, J., Lake, L.W., and Johns, R.T. (2003). Estimation of True Dispersivity in Field-Scale Permeable Media. *SPE J. 8 (3): 272–279. SPE-86303-PA. <http://dx.doi.org/10.2118/86303-PA>.*
- Manz, B., Gladden, L. F., and Warren, P. B. (1988). Flow and Disperion in Porous Media: Lattice-Boltzmann and NMR Studies. *AICE J.*, 45, 1845–1854.
- Mattax, C. C., Dalton, R. L. (1990). *Reservoir Simulation*. Richardson, TX: Henry L. Doherty Memorial Fund of AIME SPE.
- Notodarmojo, S., Ho, G. E., Scott, W. D., Davis, G. B. (1991). Modelling phosphorous transportin soils and groundwater with two-consecutive reactions. *Wat. Res.*, 1205-1216.
- Ogata, A. and Banks, R. B. (1961). *A Solution of the Differential Equation of Longitudal Disperion in Porous Media*. U.S. Geological Survey: Professional Paper 411-A.
- Olaoluwa O. Adepoju, Larry W. Lake, Russell T. Johns. (2012). Investigation of Anisotropic Mixing in Miscible Displacements. *SPE 159557*. San Antonio, Texas, USA.

- Patterson, A., Dionfrio, A., Allain, C., and Hulin, J. P. (1996). Tracer Dispersion in Polymer Solution Flowing through a Double Porosity Porous Medium. *J. Phys. II*, 6, 1639–1654.
- Pickens, J.F. and Grisak, G.E. (1981). Modeling of scale-dependent dispersion in hydrogeologic systems. . In *Water Resour. Res.* 17 (6): (S. 1701–1711).
- Simpson, E. S. (1969). Velocity and the Longitudinal Dispersion Coefficient in Flow through Porous Media. In D. Wiest (Hrsg.), *Flow through Porous Media* (S. 201–214). New York: Academic.
- Taylor, G. (1953). Dispersion of soluble matter in solvent flowing slowly through a tube. *Proc. R. Soc. Ser. A* 219, 186-203.
- Warren, J.E., Price, H.S. (1961). Flow in heterogeneous Porous Media. *Society of Petroleum Engineers Journal*, 153-169.
- Willemsen, A. (1992). *Coupled geochemical transport model*. Int. Energy Agency, Annex 7, Subtask A, in press.